INTERACTIONS BETWEEN LIGHT MESONS AND ATOMIC NUCLEI

Thesis Submitted by

NICHOLAS R.S. TAIT,
B.Sc. (Edinburgh)

for the degree of

Doctor of Philosophy

University of Edinburgh,

September, 1960.

C O N T E N T S

C O N T E N T S (Contd)

C O N T E N T S (Contd.)

Preface

The research described in this thesis has been carried out in the Department of Natural Philosophy of the University of Edinburgh under the joint direction of Professor N. Feather, F.R.S., and Dr. G.R. Evans.

CHAPTER I

INTRODUCTION

The present experiments were based on observations made during the study of cosmic rays with a cloud chamber containing 75 atmospheres of argon. On the photographs obtained were examples of the decay of positive and negative μ-mesons into positrons or electrons:

$$\mu^{\pm} \longrightarrow e^{\pm} + \nu + \bar{\nu} \quad .$$

ν and $\bar{\nu}$ are a neutrino and an anti-neutrino.

The energy spectrum of the positive and negative electrons has been determined with some accuracy. The spectrum has a maximum at an energy of 40-50 Mev and none of the particles have an energy of more than 53 Mev.

Negative μ-mesons can also undergo nuclear absorption in which case the decay process does not take place. Nuclear interactions of negative μ-mesons are discussed in rather more detail in a later chapter, but it can be stated here that in argon approximately 25% of the particles decay and the remainder are absorbed.

Examination of the photographs revealed 26 decay events. The number of nuclear absorption events was not noted but can be calculated. It is known that 20% more

positive μ-mesons enter the chamber than negative μ-mesons, while 25% of the negative particles decay. Hence it is calculated that 22 positive μ-decays, 4 negative μ-decays and 12 negative μ-absorption events are present on the film.

The number of decay electrons expected with energy less than 5 Mev for a total of 26 decay events is 0.05. Three were found,[1] having energies (2.6 ± 0.1) Mev, (3.9 ± 0.9) Mev and (2.9 ± 0.1) Mev. In the last case, observation of the direction of curvature of the particle trajectory in a magnetic field indicated that the particle was negatively charged.

It is most unlikely that these are μ-decay events and other interpretations have been considered as follows:

(i) Capture of a negative μ-meson into an extra-nuclear orbit. The binding energy of the ^1s state for a μ-meson in argon is approximately 1 Mev and if an Auger electron is emitted as a result of μ-capture this is the greatest energy it can have. The electrons cannot therefore be Auger electrons.

(ii) Capture of the μ-meson by an argon nucleus. The meson interacts with a proton in the nucleus forming a neutron and a neutrino[2]: $\mu^- + p \longrightarrow n + \nu$. Most of the excess energy (due to the large mass difference between the meson and the neutrino) is

removed by the neutrino. If only the neutrino is emitted the reaction in argon is

$$A^{40} + \mu^- \longrightarrow Cl^{40} + \nu$$

or $A^{40}(\mu^-, \nu)Cl^{40}$.

It is also possible for one or more neutrons to escape in which case Cl^{39}, Cl^{38} etc. are formed. The energies of the electrons are consistent with a line spectrum which might suggest that these particles are conversion electrons resulting from the formation of the chlorine isotope in an excited state. The emission of conversion electrons cannot compete with internal pair production at 2-3 Mev however, and no examples of double electron emission were observed.

If the events are caused by nuclear absorption of negative μ-mesons, the electrons must be produced by the decay of an isotope of Chlorine. Inspection of the photographs of the three cosmic ray events indicates that the delay between the stopping and absorption of the μ-meson and the emission of the electron was less than 100 milli-seconds, the smallest time difference detectable by observation of the thickness of the tracks. It can be assumed that the decay half life is of this order of magnitude or less. Inspection of the most recent information on the β-decay of isotopes of

Chlorine reveals no report of a half life less than 1.4 minutes.(3) This half life was reported by Morinaga for Cl^{40}.

It is possible however that an isomeric state of one of the Chlorine isotopes might exist from which β-decay might compete with γ-emission to the ground state. The β half life can be considerably shorter than that from the ground state and this process could account for the three cosmic ray experiment events.

The experiments described in the following chapters were performed with the aim of producing and studying the β-decay. The methods used were:

(i) A repetition of the cosmic ray experiment using μ-mesons produced by a particle accelerator and using sufficient mesons to produce rather more events. The energy spectrum of the electrons emitted by the stopped mesons was examined at the low energy end for indications of a β-decay spectrum with maximum energy below 10 Mev.

(ii) Formation of Cl^{40} by means of the reaction

$$A^{40} + n \longrightarrow Cl^{40} + p$$

or $$A^{40}(n, p)Cl^{40}.$$

A search was made for the decay electrons in an attempt to identify Cl^{40} as the emitting isotope.

REFERENCES, CHAPTER I

(1) Donald and Evans: Nuovo Cim., Vol. 9, Supp. 2, 385, 1958.

(2) Wheeler : Rev. Mod. Phys. 21, 133, 1949.

(3) Morinaga : Phys. Rev. 103, 504, 1956.

CHAPTER II

THE CLOUD CHAMBER

Introduction

Early experiments on supersaturated vapours indicated that the vapour would only condense and form drops if suitable condensation nuclei were present. Some of these nuclei were found to be small dust particles, but when these were removed condensation was still found to occur.

In experiments carried out by Wilson[1], [2] between 1897 and 1899, it was shown that there are two critical degrees of supersaturation in a dust-free volume. At the lower of these, condensation starts to take place on ions, while above the higher one it takes place on uncharged aggregates of molecules. Thus if the degree of supersaturation is maintained between these two values, condensation takes place on ions but not on molecules. A charged particle moving through the sensitive volume produces ions along its trajectory and under these conditions the droplets formed on the ions form a visible track in the volume.

This preferential condensation is utilised in the cloud chamber. Supersaturation is produced by cooling a mass of gas saturated with a suitable condensant, by

means of an adiabatic expansion. In a volume defined chamber, that is one in which the gas is made to expand from volume v_1 to a larger volume v_2, the ratio v_2/v_1 is known as the expansion ratio. The magnitude of the expansion ratio required to supply a given degree of supersaturation is a function of both the gas in the chamber and the condensant being used.

The ions formed during the passage of a charged particle through the cloud chamber gas diffuse away from their points of formation until the motion is arrested by drop formation. If the ions are formed some time before condensation takes place, the tracks are very broad and their edges are not well defined. A heavy background of old tracks is not desirable and an electrostatic field is applied across the gas in the chamber during the time between expansions to remove these ions. This field is normally removed before an expansion takes place.

Two classes of track are made use of in Cloud Chamber studies. Post-expansion tracks, that is, tracks that are due to particles passing through the chamber after the expansion has taken place, have the advantage of being sharp and well defined. This is because the ions diffuse only a short distance from their points of formation before being fixed in space by drop growth. Pre-expansion tracks are more diffuse and may be double

if formed while the clearing field is still on. This is due to the separation of the positive and negative ions by the field. Since there is a net gain of heat by the gas-vapour mixture during the expansion and subsequent recompression, it is necessary to allow the mixture time to cool down and attain a uniform temperature before another expansion is made - this re-cycling time will be referred to again.

A permanent record of the tracks present at each expansion can be made by taking photographs. There is a time delay between expansion and the taking of the photograph in order that the drops may grow to a suitable size. The use of two lenses giving stereoscopic views of the tracks allows a re-construction of the tracks in space to be made. (See Chapters V and X).

The High Pressure Cloud Chamber

The expansion cloud chamber that was used in the present series of experiments[3] is cylindrical in shape with internal diameter 23 cms and depth 23 cms. It is made of 'Weldanka P' non-magnetic stainless steel, the walls being 8 cms thick. These walls accommodate insulated plugs through which are passed the connections to the clearing-field electrodes, a source window used for the introduction to the chamber of particle beams,

and three armour plate glass windows through which light from Mullard L.S.D. 7 photoflash tubes passes.

The front window, also of armour plate glass, is 21 cms in diameter and 4 cms thick. The interior of the chamber is viewed through this window by a camera situated 25 cms away. The camera has two lenses of focal length 35 mms placed 7.5 cms apart. The lenses are set with their optic axes parallel and in the horizontal plane containing the chamber axis. They are operated at f/8 or f/11, and the film used was Ilford 5 G 91 35mm film.

Expansion of the chamber is effected by the movement of a rubber diaphragm between two perforated brass plates, the separation of which defines the expansion ratio. This can be altered by moving the one plate relative to the other. Prior to an expansion the diaphragm is held hard against the plate nearer to the front of the chamber by the application of a forward differential pressure of about 2 atmospheres across it. The pressure of the gas behind the diaphragm is then suddenly reduced by expansion of the gas into a large cylinder known as the expansion cylinder. The diaphragm moves rapidly back until held hard against the other plate by a differential pressure of about 10 atmospheres. It is necessary to ensure that the differential pressures are not too large because of the possibility of damaging the diaphragm.

It is necessary to allow sufficient time between expansions for the gas-vapour mixture to cool down and attain a uniform temperature. With pressures of the order of 60 atmospheres at which the present chamber is operated this re-cycling time is 15 minutes. The re-cycling time was successfully reduced to 2 minutes[4] by employing the technique of fast re-compression. The chamber gas is rapidly re-compressed by driving the diaphragm forward with gas from a high pressure reservoir, the recompression cylinder. Re-compression takes place immediately after the photographic flash, and the delay between expansion and re-compression is five hundred milli-seconds, as time must be allowed for drop growth before the tracks can be photographed. This time is kept to a minimum, however.

In Fig. 1, E is the expansion cylinder and R the recompression cylinder. The pressure cycle can be represented as follows:

(a) Diaphragm forward, v_1 and v_2 closed, $P_F = 60A$,

$P_B = 62A$, $P_E = 40A$, $P_R = 100A$.

(b) v_1 opens and diaphragm moves back.

$P_F \simeq 55A$, $P_B = P_E = 40A$.

(c) v_2 opens driving diaphragm forward, after which

$P_F = 60A$, $P_B = 62A$, $= P_E = P_B$

(d) v_1 closes and pumpforces oil into E until

$P_E = P_A = 100A.$

(e) v_2 closes and oil is let out until $P_E = 40A.$

A discussion of the development of the fast re-compression technique is given in the Appendix.

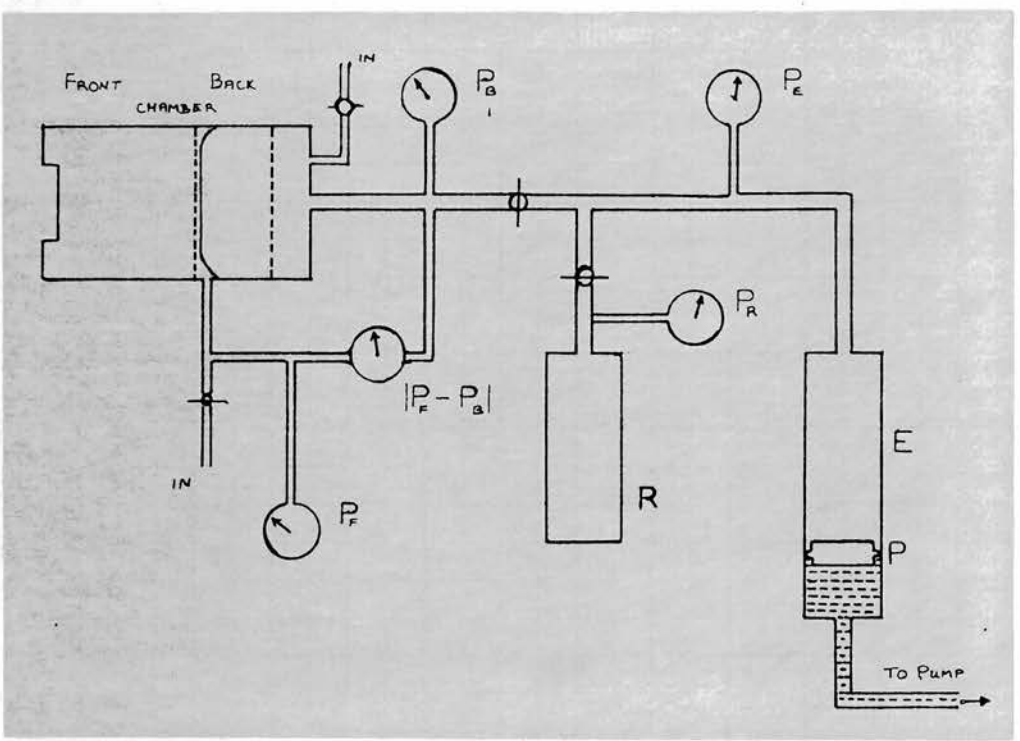

FIG. 1

This cycle takes about 1 minute to complete and there is a delay of 1 minute after this to make up the 2-minute re-cycling time before the next expansion takes place. It must be noted that if v_1 should open during (d) a very large differential would be applied across the diaphragm.

Other actions necessary during each expansion cycle are as follows:

(a) Removal of the clearing field before expansion,

(b) Operating the flash tubes at a given time after expansion,

(c) Winding on the film in the camera after exposure,

(d) Re-application of the clearing field.

These, and the elements of the pressure cycle are performed automatically by control circuits constructed by Dr. R.A. Donald.

The central component of the control circuits is a uniselector. This consists of two banks of terminals arranged around the circumference of a circle. Associated with each bank is a rotating contact which touches each terminal in turn. The moving contacts move forward one terminal each time the uniselector coil is energised and because of the placing of the terminals on the circumference of a circle, rotation through 360° makes the moving contacts return to touch the same terminal. One bank of fixed terminals is used to operate relays which perform the various actions necessary in each expansion cycle. The other bank is used to control the time separation of the elements - this depends on the length of time the moving contacts touch each terminal, and this in its turn is controlled by a thyratron timing circuit. The uniselector is activated either by the timing action of this thyratron or by connecting the grid of the valve to earth. This latter method is used

in the pumping cycle where a float in the oil pump indicates the positions of P at (a) and (b). Movement of the float is made to connect microswitch contacts which earth the thyratron grid.

The Warning Systems

It was intended to operate the cloud chamber in conjunction with particle accelerators in which case it would not be possible to remain near the chamber while the accelerating machine was in action. For this reason it was considered desirable to build a warning system that would indicate irregularities in the pressure cycle, particularly increases in the differential pressures across the diaphragm. Two systems were constructed.

(a) The Micro-switch Warning System.

This system makes it impossible for the pump to start during the cycle unless the expansion valve is closed. The pump is switched on and off by means of an A.C. relay with oil immersed contacts. The current through this pump relay is switched on either by the 'start' button situated on the pump, or by a relay in the chamber control circuits (relay 8 Fig. 2). It is switched off by the 'stop' button on the pump or by one of the float controlled microswitches.

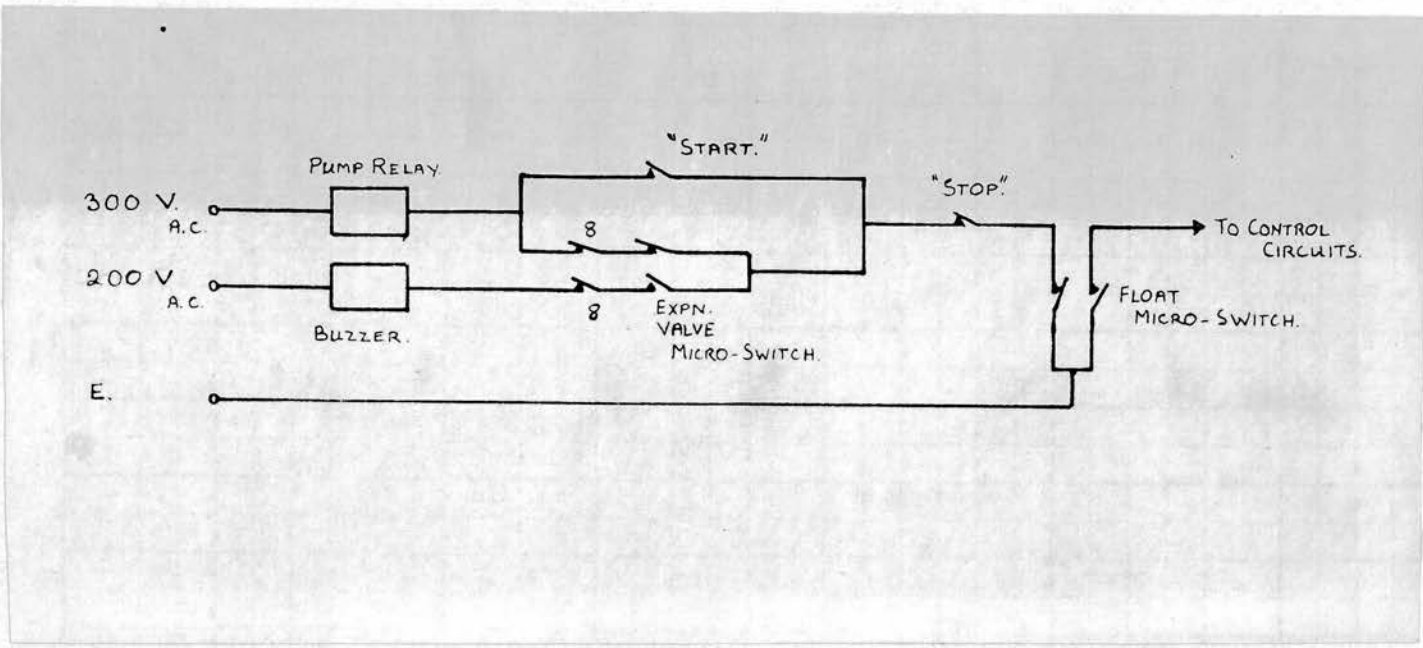
300 V.
A.C.
200 V
A.C.
E.
PUMP RELAY
BUZZER.
"START."
8
8
EXPN.
VALVE
MICRO-SWITCH.
"STOP."
TO CONTROL
CIRCUITS.
FLOAT
MICRO-SWITCH.

Fig. 2.

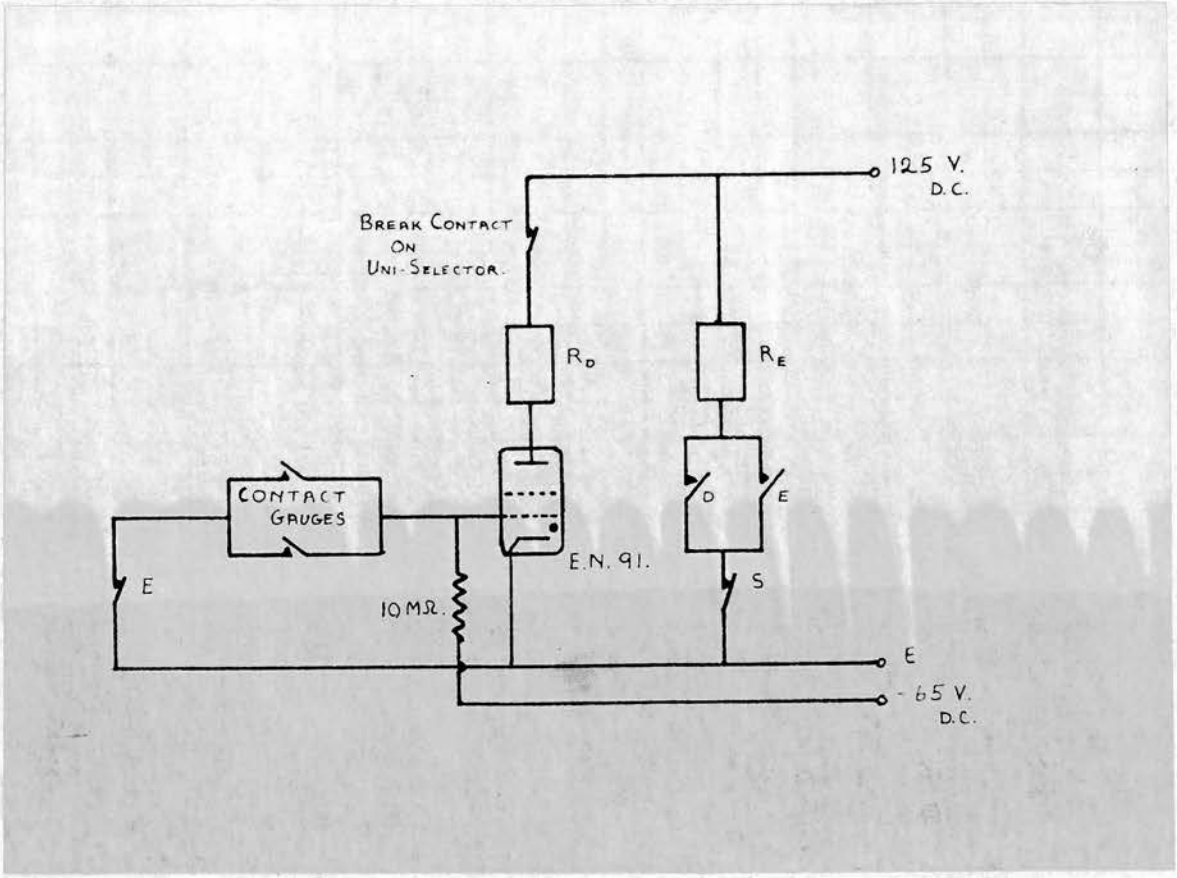
125 V.
D.C.
BREAK CONTACT
ON
UNI-SELECTOR.
R_D
R_E
CONTACT
GAUGES
E
10 MΩ.
E.N. 91.
D
E
S
E
- 65 V.
D.C.

Fig. 3.

The pump relay current is now also made to pass through a micro-switch, the contacts of which are only closed if v_1 is closed. As in the case of other micro-switches used in the control circuits this micro-switch has one 'common' terminal associated with one 'normally made' and one 'normally broken' contact ((a) and (b) respectively). Contact (b) is included in the pump relay circuit and the micro-switch arm is moved by the closing of the expansion valve. Contact (a) is used to operate a warning buzzer which starts any time when relay 8 is energised while v_1 is open.

It must be noted that the 'start' button is independent of the micro-switch system so it is possible when necessary to operate the pump with v_1 open.

It was found, on testing this system, that it is possible for v_1 to be very slightly open without the warning system coming into action.

(b) <u>The Contact Gauge System</u>.

Continuous application of the pressure cycle raises the temperature of the gas in the expansion and re-compression cylinders. Since the pressure cycle control is volume defined by means of the pump oil level, this temperature rise can result in the pressure in the re-compression cylinder becoming dangerously high and in the forward differential pressure increasing. The

contact gauge system indicates faults of this type and also overcomes the defect of the micro-switch system.

Pairs of contacts, normally not connected, are situated in the pressure gauges on the chamber. If touched by the gauge pointer the contacts are connected. Two sets of these contacts are in use - one in the gauge that measures the pressure differential across the diaphragm, in this case set to connect if a forward differential of more than 4 atmospheres is reached, and one in the gauge measuring the recompression pressure and set at 130 atmospheres.

Connection of either pair of contacts earths the grid of a thyratron which is normally kept in a non-conducting state by a negative grid bias (see Fig. 3).

This starts the thyratron conducting and relay D is energised. The closing of contacts D energises relay E while a second pair of contacts moves the uni-selector on one position. The break contacts on the uniselector immediately extinguish the thyratron discharge but relay E remains energised because contacts E(i) are closed. Contacts E(ii) ensure that the earth connection of the thyratron grid is not re-established. (The uniselector break contacts are a pair of contacts which are momentarily broken each time the uniselector coil is energised).

Relay E also starts a warning buzzer and stops

the chamber from starting another expansion cycle. The warning system is reset by de-energising relay E by means of the spring-loaded toggle switch S.

If contact is made in one of the gauges the pump is immediately stopped by the uniselector moving on, and the pressure is automatically reduced, this being the next function of the control circuits. Another expansion cannot be made until the warning system is reset.

Since these warning systems were installed water cooling has been applied to the expansion and recompression cylinders, and heating of the gas is very much reduced.

REFERENCES, CHAPTER II

(1) Wilson : Phil. Trans. 189, 265, 1897.

(2) Wilson : " " 192, 403, 1899.

(3) Donald et al. : Nuovo Cim. 4, Supp. 2, 272, 1956.

(4) Donald : Ph.D. Thesis, University of Edinburgh, 1957.

CHAPTER III

INTRODUCTION TO THE A(n, p) EXPERIMENT

The first experiment conducted with the cloud chamber described in Chapter II was an attempt to observe an isomeric state of Cl^{40} using the reaction

$$A^{40}(n, p)Cl^{40} .$$

A neutron beam with the following properties was required:

(a) The neutron energy should be higher than 8 Mev, as the threshold for the (n, p) reaction leading to the state of Cl^{40} observed by Morinaga is 6-8 Mev.

(b) The neutrons should be as nearly mono-energetic as possible so that a quantitative statement of the experimental results could be given.

With these points in view it was decided to use the $H^3(H^2, n)He^4$ reaction[1] in which a deuteron beam is made to strike a tritium target. The neutrons have an energy of 14 Mev.

The deuteron beam was supplied by the Department's particle accelerator. This is a Cockroft-Walton type accelerator in which condensers and rectifying valves are arranged in such a way that a transformer voltage is multiplied and rectified to give positive voltages of up

to 1.2 million volts. A potential difference of this magnitude is applied between the ends of a long evacuated tube. Positive ions, usually protons or deuterons, are fed into the tube at the high voltage end and accelerated to the other end which is at earth potential. Hydrogen or Deuterium is produced by the electrolysis of water or heavy water and passes into a discharge tube where it is ionised by the application of an alternating electric field of 40 Mc/s.

The ions, in this experiment deuterons, after passing down the evacuated accelerating column, are made to strike the tritium target. This target may be placed in a direct line with the main column, or the ions may be deflected by an electromagnet through an angle of 30° into one of two similar quartz tubes at the end of which the target may be situated. The quartz tubes are 1 metre long and are placed on opposite sides of the extension of the accelerating column. The tubes and the column are in the same vertical plane.

The $H^3(H^2, n)He^4$ reaction has a maximum cross-section for deuterons of energy about 100 keV[1], but it was found to be impossible to keep the deuteron beam current steady at this energy and it was necessary to increase the energy to 600 keV. for this reason.

The target, prepared by the Isotope Division, A.E.R.E., Harwell, consisted of 0.59 cc (at N.T.P.) of

Tritium absorbed in 1.9 mg. of Titanium which was evaporated onto a copper disc 0.01" thick. It was reported that the Tritium would remain absorbed almost indefinitely if the target temperature was kept below 250°, so it was necessary to use 'soft' rather than 'hard' solder to attach the copper disc to the target mounting. It was preferable to use soldering as a method of location in order to ensure good thermal contact between the copper disc and the brass mounting, the base of which contained a duct for water cooling. The water cooling was necessary particularly when the machine was being started, for during this time the beam was often striking the target continuously for several minutes.

The $H^3(H^2, n)He^4$ reaction is exothermic and most of the neutron energy is obtained from the energy release during the reaction. In the present experiment the neutrons passing through the cloud chamber were emitted at an angle of 90° to the deuteron beam while the deuteron energy was 600 keV. Under these conditions the neutron energy is 14.3 Mev. Neutrons emitted in the forward and backward directions have energies of 15.8 Mev and 12.7 Mev, and scattering of the deuterons in the target might lead to the introduction of some of these into the chamber. A small spread in the neutron energies is also expected as a result of the slowing

down of the deuterons in the target material. The lowest neutron energy expected is that corresponding to a deuteron energy of zero and is 14.1 Mev.

The deuteron beam was pulsed by application and removal of the accelerating voltage. The cloud chamber control circuits were made to operate the relays which control this voltage. The neutrons passed through the chamber from about 1 second before the expansion until after recompression. The chamber was placed with its axis at right-angles to the neutron beam. The distance from the target to the centre of the chamber was 1 metre for part of the experiment and 4 metres for the remainder. The chamber clearing field voltages used were $\pm$ 700 volts and the field was removed just before the expansion took place.

REFERENCES, CHAPTER III.

(1) Hanson et al. : Rev. Mod. Phys. 21, 635, 1949.

CHAPTER IV

THE MONITORING REACTION

The neutron flux through the chamber was monitored by adding a few atmospheres of Hydrogen to the chamber gas and observing the proton recoil tracks resulting from the collision of neutrons with hydrogen nuclei.

A neutron of energy E = 14.3 Mev and momentum p strikes a proton which is at rest. The proton recoils in a direction at angle ϕ to the trajectory of the incident neutron with energy E_p and momentum p_p, while the neutron moves off with energy E_n, momentum p_n at angle θ. The ratio β = velocity of particle ÷ velocity of light is not greater than 0.2 for any of the particles so it is sufficient to treat the mechanics of the collision non-relativistically.

Energy conservation in the reaction supplies the equation

$$E = 14.3 = E_n + E_p \qquad \text{(1)}$$

Momentum conservation along and perpendicular to the direction of the incident neutron gives

$$p = p_n \cos\theta + p_p \cos\phi \qquad \text{(2)}$$

$$0 = p_n \sin\theta - p_p \sin\phi \qquad \text{(3)}$$

In all cases the energy is proportional to the square of the momentum, assuming equal proton and neutron masses.

Hence $\cos \phi = \left(E_p / E \right)^{\frac{1}{2}}$ ———————— (4)

The maximum proton energy, corresponding to $\phi = 0$, i.e. to a head-on collision, is $E_p = E$, while the energy decreases with increasing ϕ, approaching zero as ϕ approaches $\pi/2$.

Two methods can be used to analyse the particle tracks - the method involving the reprojector, which is described in a later chapter, and the method involving direct measurement on the film, which will now be described.

Before details can be given of this method, it is necessary to define a set of co-ordinates. These are taken as follows:

Oz parallel to the optic axes of the lenses and the chamber axis.

Ox perpendicular to Oz and in the plane containing the optic axes.

Oy perpendicular to both these.

The images are thus formed in a plane parallel to that containing Ox and Oy. The origin of the system of coordinates need not be specified as the analysis requires differences of co-ordinates only.

Fig. 4 is a ray diagram in a plane containing the optic axis of one lens. Two objects O_1O_2 and $O_1'O_2'$

at distances z and z' from the pole of the lens P form images on the film at distance z" from P. These images are represented by I_1I_2 and $I_1\ I_2'$.

$$\text{Now } \frac{z}{z''} = \frac{O_1O_2}{I_1I_2}, \quad \frac{z'}{z''} = {}^{O_1'O_2'}/_{I_1I_2'}$$

$$\therefore \Delta z = z - z' = z'' \left[\frac{O_1O_2}{I_1I_2} - \frac{O_1'O_2'}{I_1I_2'}\right]$$

$$= z'' \left[\frac{1}{m} - \frac{1}{m'}\right] \text{ ——————— (5)}$$

where m and m' are the magnifications in the two cases.

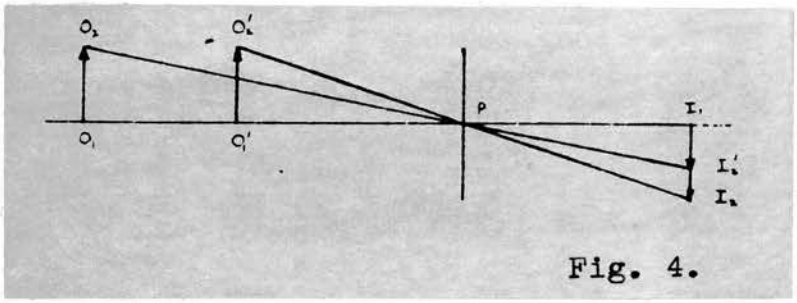

Fig. 4.

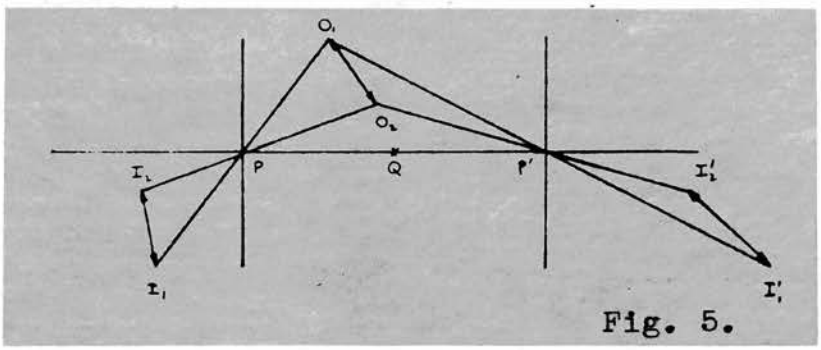

Fig. 5.

Fig. 5 is in a plane perpendicular to Oz. P and P' are the axes of the two lenses and object O_1O_2 forms images I_1I_2 and $I_1'I_2'$. The lines I_1I_1' and I_2I_2' are always parallel to PP', and I_1I_2 is parallel to $I_1'I_2'$ if the object is in a plane perpendicular to Oz. It can be shown by a method involving similar triangles

that the values of m corresponding to the ends O_1 and O_2 of the object are given by

$$m = \frac{D - L}{L} \qquad m' = \frac{D' - L}{L} \qquad (6)$$

where $D = I_1 I_1'$

$D' = I_2 I_2'$

$L = PP'$.

Now if the differences in the coordinates of the ends of a track are Δx, Δy and Δz, O_1O_2 in Fig. 5 being the projection of the track onto a plane perpendicular to Oz,

$$O_1O_2 = ((\Delta x)^2 + (\Delta y)^2)^{\frac{1}{2}}$$

The method used to find Δx and Δy in the present experiment was as follows. If X_1Y_1 and X_2Y_2 are the x and y distances of I_1 and I_2 respectively from P, then it can be shown that

$$\Delta x = {}^{1}/_{m}\left[\frac{m}{m'} X_2 - X_1\right] = \frac{L}{D-L}\left[\frac{D-L}{D'-L} X_2 - X_1\right]$$
$$\Delta y = {}^{1}/_{m}\left[Y_1 - \frac{m}{m'} Y_2\right] = \frac{L}{D-L}\left[Y_1 - \frac{D-L}{D'-L} Y_2\right] \qquad (7)$$

and a similar pair of expressions exists involving P', I_1' and I_2'. Thus if the coordinates of I_1, I_2, $I_1'I_2'$, P and P' are measured, it is possible to calculate Δx and Δy using (7), while Δz is obtained from equations (5) and (6). It is a simple

matter to find the coordinates of P and P' since the optic axes are co-planar with and equidistant from the axis of the chamber, while the distance PP' is known.

The coordinates were measured with a Cambridge Universal Measuring Machine (number C 373765). This instrument has two scales with smallest scale division 0.001 cms set at right angles to each other. The film is placed between two plane glass plates which are rotated in the plane containing the film until the image of a given feature in the chamber has the same y-coordinate in each of the photographs. The coordinates are then obtained using the microscope scales.

Before this method can be used it is necessary to know the values of the constants L and z". In order to find these a pair of photographs was obtained of an object for which Δz was known. Measurements taken from the film then gave the values of m and m' in equation (6) once L was known. This was measured with a measuring microscope, the mean of a set of ten readings being taken. Substitution of the values of m and m' obtained from (6) into equation (5) allowed z" to be evaluated. The results were:

$$L = 7.516 \text{ cms}$$

$$Z'' = 3.778 \text{ cms.}$$

A sample of the tracks were analysed in this way, but it can be seen that the process is somewhat involved

and rather slow. It was noted however that if equations (7) were applied to the view in which a track was nearer to the optic axis, the fraction $\frac{D - L}{D' - L}$ seldom differed from unity by more than 5%. If the fraction is taken equal to unity, the equations become

$$\Delta x = {}^{1}/_{m}(X_2 - X_1) = {}^{1}/_{m}\,\Delta X,$$

$$\Delta y = {}^{1}/_{m}(Y_1 - Y_2) = {}^{1}/_{m}\,\Delta Y, \quad \text{and}$$

$$O_1O_2 = \left({}^{1}/_{m}\right) I_1 I_2 \qquad \text{(8)}$$

Now O_1O_2 is the projection of the track onto the plane containing Ox and Oy while the cloud chamber was orientated relative to the target such that the trajectories of the incident neutrons were in this same plane. Thus if a method could be found of calculating the distribution of lengths of the recoil proton tracks projected onto a plane containing the incident neutrons, it would be possible to study the monitoring reaction using only equation (8) and thus reducing considerably the time taken to perform the analysis.

The projected track-length at a given angle ϕ can vary between the actual track-length R' if ϕ is in the plane of projection, to R' cos ϕ if it is in a plane at right-angles to this. In order to calculate the number of recoil protons which have a projected

track-length greater than any arbitrary length R_p' it is necessary to know:

(a) The relationship between track length R' and particle range R. Assuming a track width $\sim$ 0.1 cms, the required relationship is

$$R' = R + 0.1 \text{ cms} \qquad \text{——————} \qquad (9)$$

(b) The relationship between R and E_p. This is a function of the chamber gas, both in constitution and in pressure.

(c) The variation in the number of recoils with scattering angle, ϕ. This will be discussed later.

Corresponding to every value of ϕ there is a value of R', and if tracks of projected length greater than R_p' are being counted, two values of ϕ can be defined as follows:

ϕ_1 corresponds to $R' = R_p'$, so for ϕ greater than ϕ_1 no tracks with projected length $\geqslant R_p'$ will be seen.

ϕ_2 corresponds to $R' \cos \phi_2 = R_p'$. For ϕ less than ϕ_2 all tracks have projected length $\geqslant R_p'$. ϕ_1 is determined using range-energy data and equation (4) while ϕ_2 is found as follows: from (4)

$$\cos \phi_2 = \left(E_p / E \right)^{\frac{1}{2}} ,$$

while $R' \cos \phi_2 = R_p' = (R + 0.1) \cos \phi_2$

$$\text{i.e. } \cos \phi_2 = R_p' / (R + 0.1) .$$

These two expressions can be solved graphically for ϕ by plotting

$$F_1 = \left(E_p/E \right)^{\frac{1}{2}} \quad \text{and}$$

$$F_2 = R_p'/(R + 0.1)$$

against E and obtaining the value of E and hence also of ϕ at the intersection of the two curves.

Between angles ϕ_1 and ϕ_2 the direction of the recoil must be considered. In fig. 6, the plane of projection is OAB and if the track of length R' is represented by OE, then R_p' = OD. E can be situated anywhere on the circumference of the circle. If OC is the direction of the trajectory of the incident neutron, ϕ is the angle AOC.

Let angle ECD = θ, DOE = ψ, CE = r.

Then $\sin \psi = r \sin \theta / R'$

and $R' \sin \phi = r$,

so $\sin \phi \sin \theta = \sin \psi$.

A track is counted if

$$OD = R' \cos \psi \geqslant R_p'$$

$$\text{i.e. } (R + 0.1)(1 - \sin^2\phi \sin^2\theta)^{\frac{1}{2}} \geqslant R_p' \ .$$

The fraction $a(\phi)$ that is accepted at a given value of ϕ between ϕ_1 and ϕ_2 can be found from this expression. Thus for equality

$$\sin^2\theta = (1 - ({}^{R'}p/R + 0.1)^2)/\sin^2\phi.$$

Since there is equal probability of any value of θ between 0° and 90°,

$$a = {}^{\theta^\circ}/_{90^\circ} .$$

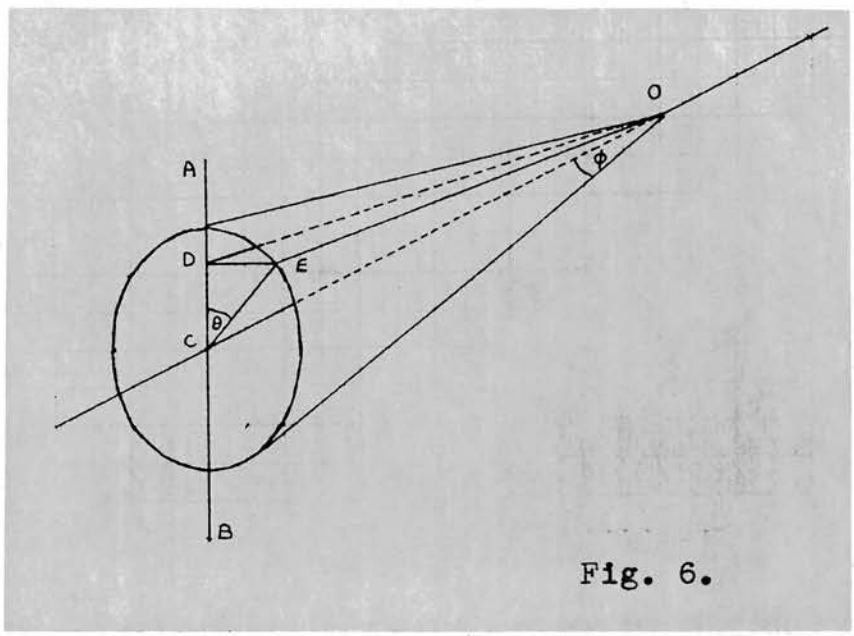

Fig. 6.

It is now necessary to know the number of proton recoils which occur at angle ϕ. Experiments indicate[1] that the distribution is isotropic in the centre of mass system of coordinates. Transformation into the laboratory coordinate system indicates that the number of recoils between angle ϕ and angle $\phi + d\phi$ is proportional to $\sin 2\phi d\phi$. If the constant of proportionality is n, the total number of recoils is

$$n. \int_0^{\pi/2} \sin 2\phi \, d\phi = n$$

$\therefore$ fraction between angles ϕ and $\phi + d\phi$

$$= \sin 2\phi \, d\phi .$$

The fraction of recoils with projected length $\geqslant R_p'$ can now be found: it is

$$\int_{\phi_2}^{\phi_1} \alpha(\phi) \sin 2\phi \, d\phi + \int_{0}^{\phi_1} \sin 2\phi \, d\phi$$

and the first integral is evaluated graphically. These integrals were evaluated for six values of R_p' and the results are given in the table. The details of the calculations are given for $R_p' \geqslant 0.3$ cms, while only the results are given in the other five cases. The fraction of the tracks with projected lengths between any two of these values of R_p' are then found by subtraction. Note that the integrals are dependent on the chamber gas pressure. The present results are for a chamber filling of argon at 58 atmospheres.

Results for $R_p' \geqslant 0.3$ cms.

ϕ	64°	62°	60°	57°
R' cms	0.3	.35	.40	.50
$1 - (3/R')^2)^{\frac{1}{2}}$	0	.516	.661	.800
$\sin \phi$	.900	.883	.866	.838
θ	0	$35^\circ\ 40'$	$49^\circ\ 40'$	$73^\circ\ 0'$
α	0	.39	.55	.81
$\alpha \sin 2\phi$	0	.326	.476	.740

Results for $x \leq R_p' < y$

The integrals were evaluated from Fig. 7.

x cms	0.3	0.5	0.9	1.5	2.0	3.0
y cms	0.5	0.9	1.5	2.0	3.0	max.
fraction	.095	.113	.132	.110	.168	.113

Reasons for the choice of these ranges of values R_p' will be discussed later in the chapter.

The observed distribution will be expected to differ from the calculated distribution for the following reasons:

(a) The presence of heavy particle tracks due to the interactions of neutrons with other nuclei. These interactions result in the recoil of the product nucleus but the recoil track is too short to be observed in the present experiment. It is sometimes possible to identify the tracks caused by such reactions by observation of their lengths.

(b) A non-parallel beam. The effect of beam divergence due to the finite distance of the neutron source from the cloud chamber should be small as the solid angle subtended by the chamber at the target was 10^{-2} or less.

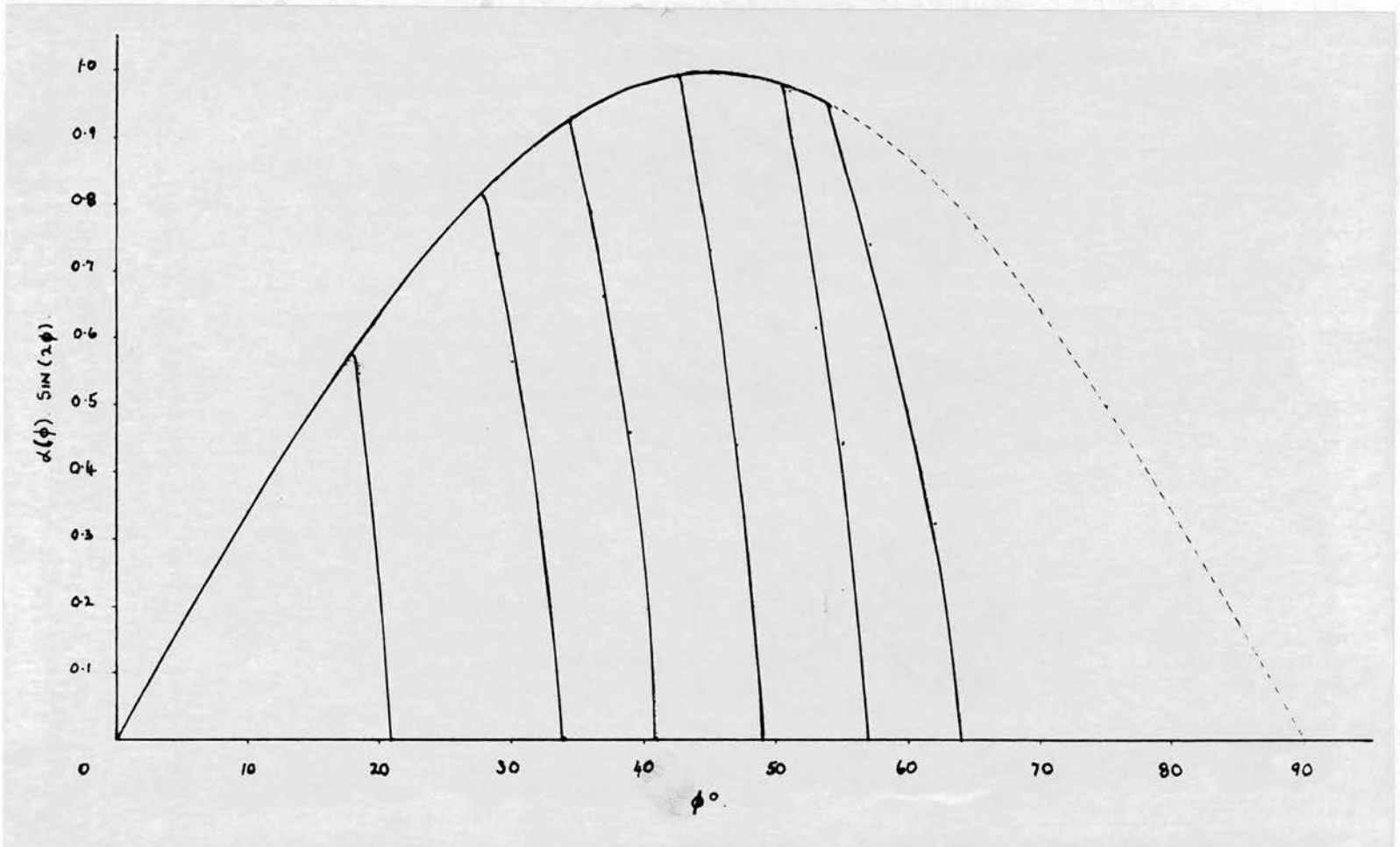

Fig. 7.

(c) Elastic and inelastic scattering of the neutrons could have a more serious effect. Neutron scattering is discussed in more detail in Chapter V.

It was realised that measurement of projected lengths would not afford detailed information about sharp peaks in the distribution of actual track lengths, but that it would give a reasonable estimate of the neutron flux. Accordingly, the projected lengths were classified in the broad range groups discussed earlier such that the number of monitor reaction events expected in each group was approximately equal. The analysis process was further simplified by the use of a constant value of $^{1}/_{m}$ in equation (8). The values of $^{1}/_{m}$ obtained for the tracks in the sample analysed by the detailed method were:

$\frac{1}{m}$	7.2-7.5	7.6-7.9	8.0-8.3	8.4-8.7	8.8-9.1	9.2-9.5	9.6-9.9
number	5	17	5	15	9	8	4

The mean value of $\frac{1}{m}$ is 8.4 while the spread in the values is not large so it was expected that the assumption of constant $\frac{1}{m}$ would have little effect on the observed distribution when the scheme of broad range groups with approximately equal numbers in each group was used. Comparison of the true projected lengths

obtained for the sample of tracks using equation (7) with the lengths obtained using equation (8) and the mean value of $\frac{1}{m}$ is made in Chapter VI.

It was necessary to study the heavy particle tracks due to other neutron reactions in the chamber gas before a reliable interpretation could be given of the experimental results. These tracks were studied using data obtained from the sample, using the detailed method of analysis.

Measurement of the track length on the film was made using a glass scale with 0.1 mm scale divisions. This was held over the track image on the view in which the image was nearest to the optic axis and was examined under a x 10 magnification. The lengths on the film could be measured to $\pm$ 0.5 of the smallest scale division corresponding to $\pm$ 0.04 cms in the full size projected track length.

REFERENCES: Chapter IV

(1) Barschall et al. Phys. Rev. 75, 1819, 1949.

CHAPTER V

PARTICLE TRACKS IN THE CHAMBER

The events for which the photographs taken in this experiment were being scanned were those due to the $A^{40}(np)Cl^{40}$ reaction followed by the decay $Cl^{40} \longrightarrow A^{40} + e^- + \nu$. It was anticipated that the nuclear recoils would not be observed so the events would consist of a proton track associated with an electron track, the proton and the electron both having energies of less than about 15 Mev. It was therefore essential to be able to distinguish between the tracks of protons and electrons below this energy. Several of the expressions quoted in this chapter are only approximate, but they are sufficient to demonstrate that this discrimination is possible in the high pressure cloud chamber. Three properties of particles and their tracks will be considered:

(a) Track thickness.

If the average energy loss per ionising collision for a given particle in a given medium is taken to be independent of the particle energy, then

$$dn/dx \propto \left| dE/dx \right| \quad \text{, where}$$

dn_{dx} = number of ions formed/unit path length

$-dE/dx$ = energy lost/unit path length,

while $-dE/dx \propto \frac{Z^2}{\beta^2} f(\beta, \omega)$ where

Z = charge of ionising particle,

β = velocity of the particle relative to the velocity of light,

and ω = maximum possible energy transfer from the ionising particle to a free electron. ω is inside a logarithmic term however and its variation is neglected here. The rigorous expression is discussed in detail in reference (1).

Neglecting the variation of f with ω, it can be seen that at the same β-value, $\left|dE/dx\right|$ will be four times as large for an α-particle as it is for a proton.

The ions can all be considered to be formed exactly on the trajectory of the ionising particle. The ions diffuse away from their points of formation so that after time τ, the density of these ions at distance r from the particle trajectory is given, neglecting re-combination, by[2]

$$p(r) = N_o/4\pi D\tau \; e^{-r^2/4D\tau}$$

where D = diffusion coefficient

N_o = number of ions/unit track-length $= dn/dx$.

The diffusion process is eventually stopped by the formation of drops on the ions. The expression cannot easily be used to predict the density of drops in the track after drop growth is complete for several reasons:

(i) The diffusion coefficient is a function of temperature and the temperature varies during expansion and drop formation.

(ii) The ratio (number of drops) ÷ (number of ions) is not equal to unity. Further it varies with the ion density.

There are two further processes that take place before the track is observed:

(i) Light from the electronic flash tubes is reflected from the tracks; variation of the intensity of the reflected light with drop size and density is expected. It is not possible to predict this variation especially since the problem is further complicated by variation of intensity with the angle of scattering.

(ii) The scattered light falls on the film in the camera; in order to predict the appearance of the track image it is necessary to know how the blackening of the film varies with the intensity of the incident light.

Observation of the images of tracks formed in a high pressure cloud chamber with $\tau \sim 1$ second shows that the edges are well defined and that the apparent track thickness varies between 0.03 cms for particles with $\beta \sim 1$ and $-dE/dx$ small, and 0.10 cms for particles with small β-values. The difference in track thickness for large and small β-values is very small in the case of post-expansion tracks.

(b) Particle Range R.

For heavy particles

$$R = \frac{m}{Z^2} G(\beta), \quad \text{where}$$

$G(\beta)$ is a function of β only.

At a given energy an electron has a considerably greater range than a proton. This is only true while electron energy losses due to the emission of electro-magnetic radiation are small compared with ionisation losses which is certainly so for electrons of energy less than 15 Mev in Argon or Nitrogen. At the same energy an α-particle has a shorter range than a proton.

Owing to its smaller mass, an electron has a higher β-value than a proton of the same energy. Thus since $-dE/dx$ decreases with increasing β the rate of loss of energy of the electron is less than that of the proton and its track width is smaller also. (In fact, rate of energy loss decreases with increasing β, reaches a minimum and then rises again to reach a steady value slightly above minimum. This increase is scarcely detectable by observation of track thickness however).

An electron track with $\tau \sim 1.0$ seconds has a width of approximately 0.03 cms up to 2 mm. residual range. The track width increases rapidly to about 0.10 cms within the last two millimetres and an electron

stopping in the chamber gas can be identified by means of the 'blob' of heavy ionisation at the end of its range. In the case of a proton, the track thickness is almost constant over the last 4 cms of the particle range.

The thickness over the last 4 cms for $\gamma \sim 1.0$ secs is about 0.10 cms.

(c) Multiple Coulomb Scattering.

This is discussed in detail in Chapter IX. It is sufficient to say here that the root mean square angle of scattering in a given medium is given approximately by the expression

$$\left(\overline{\phi^2}\right)^{\frac{1}{2}} = k/p\beta \quad \text{where}$$

k = constant for given scattering material,

p = momentum of scattered particle.

Under the conditions of the present experiment little evidence is found of multiple scattering on the tracks of protons. The last 10 cms of an electron track exhibit much multiple scattering and the direction of travel of the electron can sometimes be determined by observation of an increase in the scattering as the electron slows down and $p\beta$ decreases even if the end is not visible.

The track of an electron of a few Mev energy can be distinguished from that of a proton by observation

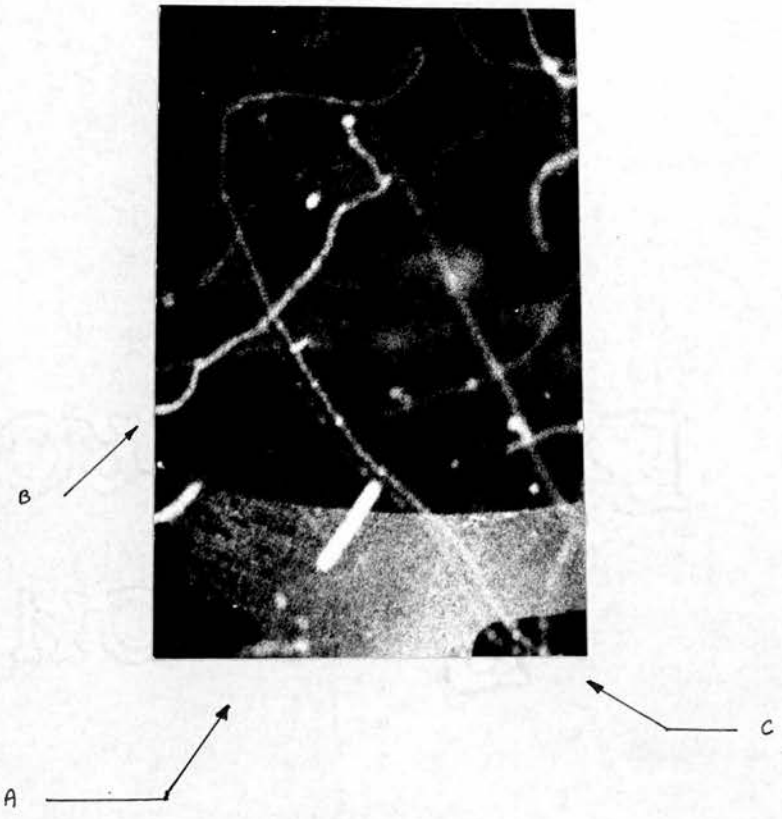

PLATE 1

A is the track of a proton of range 0.7 cms and energy 5.6 Mev. B is the track of an electron which stops in the chamber gas. The 'blob' of ionisation at the end of the particle range can be seen clearly. The range of the electron is ~2.5 cms corresponding to a minimum energy of 0.96 Mev.

Track C is the track of an electron of somewhat higher energy passing through the chamber and not stopping. The separation of the positive and negative ions by the electric field is seen on this track. The difference in intensity of the two parts of the track is due to the preferential condensation of ethyl alcohol on positive ions. The electron energy is greater than 1.3 Mev.

of track thickness alone in the present experiment. Meson and proton tracks can be distinguished by the greater degree of multiple scattering near the end of the range of the meson.

Typical proton and electron tracks can be seen in plate 1.

Contents of the Photographs

The 14 Mev neutrons entering the cloud chamber interact with the nuclei of the various elements present to give heavy particle tracks. The fraction of the tracks contributed by the different reactions depends in each case on the number of nuclei present and on the reaction cross-section σ. Thus if N neutrons enter the chamber which contains n_x nuclei of element x, the number n of heavy particle tracks resulting from a reaction which has a cross-section σ is

$$n = N n_x \sigma \qquad \text{(1)}$$

The number of molecules in 1 cubic centimetre of gas at N.T.P. is a constant - Avogadro's number, 2.69×10^{19}. The number of molecules in 1 cc at temperature $T^{o}A$ and pressure p atmospheres is $2.69 \times 10^{19} \times p \times \frac{273}{T}$. All the gases in the chamber with the exception of Argon are diatomic and equation (1) becomes

$$n = N \times 2 \times 2.69 \times 10^{19} \times p \times \frac{273}{T} \times \sigma \ ,$$

or for a diatomic gas at a given temperature

$$n = N\, kp\sigma \qquad \text{——————} \qquad (2)$$

For Argon and other monatomic gases this becomes

$$n = N\, \tfrac{1}{2} kp\sigma \ ,$$

where k is a constant.

The energy of the charged heavy particles emitted in each reaction can be calculated using equations similar to equations (1) - (3) of Chapter IV. Two equations are obtained for conservation of momentum and one for the conservation of energy. In most cases energy is released during the reaction so equation (1) of Chapter IV becomes

$E_1 + E_2 = E + Q$, where

Q = reaction energy which may be negative,

E_1 and E_2 are the energies of the heavy particle and the product nucleus. The heavy particle has maximum energy when it is emitted along the direction of the incident neutron and minimum energy when emitted at 180° to this direction. The ranges corresponding to these energies can be obtained from the appropriate range-energy curves for protons, the expression quoted in (b) above being used if the heavy particle is not a proton. The proton range energy

curves used in the present experiment are given in Fig. 8.

The difference between the maximum and minimum heavy particle energies is frequently not large and the reaction responsible for a group of tracks can frequently be identified if the energy of the particles is found to be consistent with the known Q-value of the reaction. For any given reaction there will be a series of groups corresponding to the formation of the product nucleus in the ground state, the first excited state and so on. If the excited states are close to the ground state, however, it is not always possible to distinguish the resultant groups. Reaction Q-values are normally quoted for the reaction leading to the formation of the product nucleus in the ground state.

The heavy particle tracks can conveniently be divided into two categories:

(a) Heavy particle tracks with associated electron track. These will result from a neutron-heavy particle interaction leading to the formation of a nucleus which emits a β-particle. Suppose the half-life of the β-decay is τ' and suppose that at time $t = 0$, N_o radio-nuclei are present. After time t the number that have decayed is N, where

$$N = N_o(1 - e^{-t/\tau'})$$

i.e. fraction that decay is given by

$$f = (1 - e^{-t/\tau'}).$$

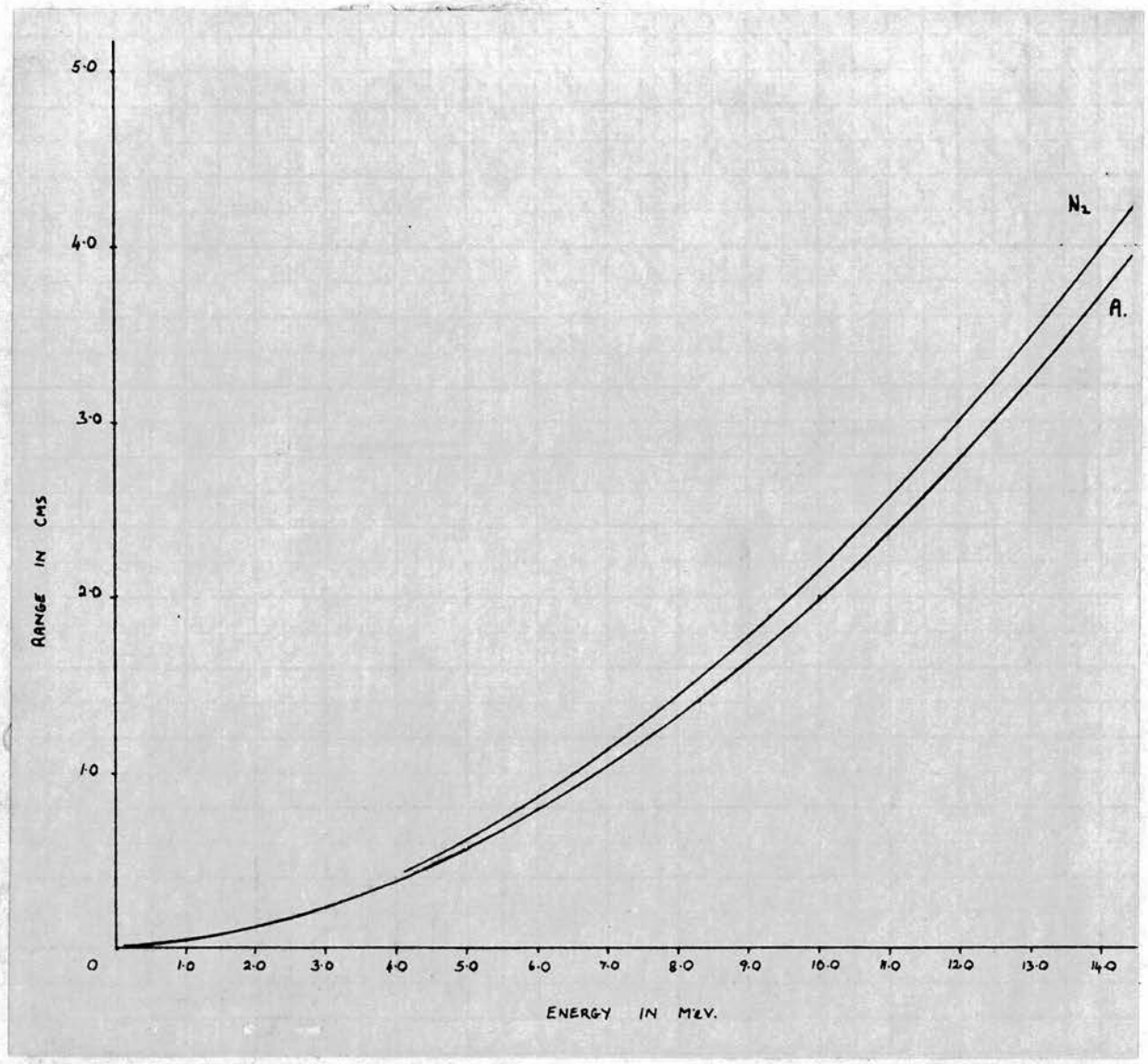
5·0
4·0
3·0
2·0
1·0
0
RANGE IN CMS
1·0
2·0
3·0
4·0
5·0
6·0
7·0
8·0
9·0
10·0
11·0
12·0
13·0
14·0
ENERGY IN MEV.
N2
A.

Fig. 8.

If, as in the present experiment there is continuous production from time $t = 0$ until the time of observation,

$$f = \int_0^t (1 - e^{-t/\tau'}) \, dt \quad .$$

The neutron beam started to enter the chamber about 1 second before the expansion took place, and since only pre-expansion tracks were being considered,

$$f = \int_0^1 (1 - e^{-t/\tau'}) \, dt$$

$$= 1 - \tau'(1 - e^{-1/\tau'})$$

$$= \tfrac{1}{2}\tau' \quad \text{if } \tau' \gg 1.$$

Hence for the consideration of reactions leading to a β-active product nucleus where the electron track is observed, equation (2) must be modified such that

$$n = Nkp\sigma f. \qquad \text{(3)}$$

(b) Heavy particle tracks without associated electron track.

A fraction (1 - f) of the radio nuclei discussed in (a) contribute to this group. There are also contributions from reactions leading to the formation of a stable nucleus.

The heavy particle tracks in (a) and (b) are mainly due to (n,p) and (n,α) interactions. In the results of Chapter VII only these types of reaction have been listed. No significant contribution is

expected from reactions such as (n,d) or (n,np) as all those concerned have small cross-sections.

Neutron Scattering

This has an effect on the distribution of projected track lengths in the monitoring reaction. The scattering is of two types - elastic and inelastic. If a neutron is scattered elastically, the scattering nucleus is left in the ground state and the reaction energy Q is zero. Inelastic scattering leaves the nucleus in an excited state and Q can have a series of negative values corresponding to different excitation energies of the scattering nucleus. Three sources of scattered neutrons will be considered. Scattering in the target holder has been neglected.

(a) Scattering in the chamber walls.

The walls are 8 cms thick. The elastic and inelastic cross-sections for 14 Mev neutrons in Fe are both approximately 1.2 Barns.(3),(4)

A 14.3 Mev neutron scattered elastically at $\phi = 180^{\circ}$ from an iron nucleus will have an energy of about 13.4 Mev. It is assumed that all the neutrons in the direct beam pass through 8 cms of iron before entering the chamber gas.

The number of atoms of iron in 56 gms = 6.03×10^{23}
Taking the density of iron as 8 gms/cc,

Number of atoms/cc $= 6.10^{23}.8/56 = \frac{6}{7} . 10^{23}$

Thus the number of interactions (elastic or inelastic) for each neutron in passing through 8 cms of iron

$$= \frac{6}{7} . 10^{23} . 8 . 2.4 .10^{-24}$$

$$\sim 1.7 .$$

Half these will be elastic interactions, the scattered neutron having a maximum energy of 14.3 Mev and minimum energy $\sim$ 13.4 Mev. The remainder will be inelastic interactions. Fe^{56} has several levels with excitation energy less than 3 Mev[5] corresponding to a minimum neutron energy of about 10 Mev, but the probability of leaving the Fe nucleus in the different excited states is not known so no energy distribution can be quoted for the inelastically scattered neutrons.

The neutrons scattered in the chamber walls will effect the distribution of projected track-lengths in the monitoring reaction in two ways: firstly because of the neutron energy change. The distribution of the H(n,p) tracks for a neutron energy 13.0 Mev has been calculated - the results are compared with those for 14.3 Mev neutrons below:

E_p \ R'_p	0.5-0.9 cms	2.0-3.0 cms	3.0-Max. cms.
14.3 Mev	.113	.168	.113
13.0 Mev	.119	.14	.03

The change in the distribution can be seen to be large for the longer tracks but very much smaller below $R'_p = 0.9$ cms.

The scattering also alters the neutron directions - it is not possible to estimate the effect that this will have on the distribution.

(b) Scattering in the walls, floor and ceiling.

These were of concrete which contains elements of smaller atomic number. For an element with $A \sim 15$ the energy of a 14.3 Mev neutron scattered at $\phi = 180^{\circ}$ is about 10.6 Mev. The scattering cross-section (elastic and inelastic) in this region is $\sim$ 1.5 Barns, while the number of atoms per cc $\sim 10^{23}$. The distances between nuclear energy levels near the ground state in nuclei of elements in this region are mainly 0.5-2.0 Mev so the inelastic scattered neutrons will have significantly less energy than those that are scattered elastically while the energy loss for elastic scattering is greater at $A \sim 15$ than at $A = 56$.

The contribution from this source would be expected to be at somewhat lower energies than the contribution from (a), but the magnitude of the contribution cannot be assessed.

(c) The Electro-magnet core.

This was situated 1 metre vertically above the neutron source while the line joining the source to the chamber was approximately horizontal. The energies

of the scattered neutrons will be the same as in (a) but the numbers will be smaller because of the smaller solid angle subtended by the chamber at the magnet.

There was a possibility of significant contributions to the short R_p' groups from long tracks due to interactions involving neutrons scattered at angles of the order of 90°. Measurement of the actual rather than the projected lengths for a sample of tracks using the method discussed in Chapter IV indicated no such significant contribution.

The distribution of projected track lengths has been observed for different neutron source - cloud chamber separations in an attempt to assess the effects of (b) and (c).

REFERENCES: Chapter V

(1) Rossi: High Energy Particles, Prentice-Hall, 1952.

(2) Wilson: Principles of Cloud Chamber Technique, C.U.P., 1951, p. 67.

(3) Graves: Phys. Rev. 97, 1205. 1955.

(4) Coon : Phys. Rev. 88, 562. 1952.

(5) Lloyd : Phys. Rev. 64, 321. 1948.

CHAPTER VI

RESULTS AND INTERPRETATION

Three different chamber fillings and two source-chamber distances d were used. The photographs obtained may be classified accordingly:

Run \ Gas	A	N_2	H_2	O_2	d(metres).
I	57	¾	5	¼	1
II	57	¾	5	¼	4
III	0	50	6	¼	4
IV	58	¾	$\frac{1}{12}$	¼	4

All pressures are in atmospheres. The small quantities of N_2 and O_2 present in runs I, II and IV are contained in the 1 atmosphere of air that was present in the chamber in each run. The $^1/12$ atmos. of hydrogen present in run IV is the hydrogen in the condensant alcohol which also contains carbon and oxygen.

The photographs were scanned for heavy particle tracks with or without associated electron tracks. The heavy particle tracks had to be in such positions in the cloud chamber that they were in view in both photographs and that the images on the film were in good focus.

Events consisting of a heavy particle and associated electron track were rejected if the free end of the electron track was in the chamber gas and showed no evidence of the thickening characteristic of an electron stopping. Tracks of electrons leaving the chamber were examined for evidence of increase in multiple scattering with increasing distance from the heavy particle track. The range of the heavy particle in these events was measured by the 'detailed' method of Chapter IV.

The choice of 0.3 cms for the minimum projected track length in the classification of heavy particles without associated electron leads to the exclusion of most of the (n, α) reactions. In run III where the gas pressure was lower, the minimum projected track length accepted was 0.5 cms. Electrons of energy below 100 keV have a range of less than 0.1 cms over much of which the track thickness is $\sim$ 0.1 cms. Two tracks of such electrons formed close together might under some conditions be mistaken for a heavy particle track. The choice of 0.3 cms for the shortest projected track length ensured that such mistakes were not made.

A summary of the interactions taking place in the chamber is given below - the notation is to be found in Chapter V.

It is apparent on inspection that few of the α-particle tracks will be included in the scanning so

RUNS I and II

Reaction	No.	σ m.b.	$p_{atmos.}$	Q Mev	R' max cms	γ'	f	σpf^{*}	$\sigma p(1-f)^{*}$	Refs.
$H^{1}(n,p)$	(i)	690	5	0	3.6	∞	0	0	3450	(1)
$N^{14}(n,p)C^{14}$	(ii)	150	.75	.6	4.0	∞	0	0	112	(2)(3)
$N^{14}(n,\alpha)B^{11}$	(iii)	100	.75	-.2	.35	∞	0	0	75	(2)(3)
$A^{40}(n,p)Cl^{40}$	(iv)	σ	57	-6.7	1.1	1.4m	.006	.17	29σ	(4)
$A^{40}(n,\alpha)S^{37}$	(v)	33 (?)	57	-2.0	.31	5m	.002	1.9	940	(5)
$O^{16}(n,p)N^{16}$	(vi)	100	.25	-9.4	.70	7.5S	.067	1.8	23	(2)(6)
$O^{16}(n,\alpha)C^{13}$	(vii)	300	.25	-2.3	.30	∞	0	0	75	(2)

* $\frac{1}{2}\sigma pf$ and $\frac{1}{2}\sigma p(1-f)$ in the case of argon.

RUN III

Reaction	No.	$p_{atmos.}$	R'_{max} cms	σpf	$\sigma p(1-f)$
$H'(n,p)$	(i)	6	4.1	0	4140
$N^{14}(n,p)$	(ii)	50	4.5	0	7500
$A^{40}(n,p)$	(iv)	0	-	-	-
$O^{16}(n,p)$	(vi)	.25	.84	1.8	23

RUN IV

Reaction	No.	$p_{atmos.}$	R'_{max} cms	σpf	$\sigma p(1-f)$
$H'(n,p)$	(i)	$\frac{1}{12}$	3.6	0	58
$N^{14}(n,p)$	(ii)	.75	4.0	0	112
$A^{40}(n,p)$	(iv)	58	1.1	σ .17	300
$O^{16}(n,p)$	(vi)	.25	.70	1.8	23

these have been omitted from the 2nd & 3rd tables as have details such as σ and γ'.

Heavy Particle Tracks without associated Electron Track.

It was demonstrated in the last chapter that the upper end of the projected track-length distribution is rather sensitive to the neutron energy. Since some spread in the neutron energies was expected because of neutron scattering, it was decided to normalise the theoretical distribution using all H(n,p) tracks with $R_p' \geq 2.0$ cms. It must be realised that the neutron flux estimated in this way will contain contributions from neutrons of energy less than 14.3 Mev.

In runs I and II the only reaction apart from H(n,p) which contributes at $R_p' \geq 2.0$ cms is reaction (ii). Comparison of the values of $\sigma p(1-f)$ for reactions (i) and (ii) shows that only a small fraction of the tracks in this range can be expected to be due to (ii), and in normalisation of the theoretical curve reaction (ii) has been neglected.

In run III this situation is no longer true and since the expected distribution of the projected track lengths is not known for reaction (ii) a normalisation of the theoretical distribution for (i) is not possible.

In the following tables the results of the projection measurements are given together with the estimated contribution from reaction (i) in runs I and II. The

results given for run III are for a sample of about $1/3$ of all the photographs taken.

Results of Scanning

Run \ R'_p cms	0.3-0.5	0.5-0.9	0.9-1.5	1.5-2.0	2.0-3.0	3.0- max
I	33	73	35	26	25	17
II	16	14	10	7	10	3
III	-	98	89	20	34	30
IV	4	11	3	1	2	0

Predicted H(n,p) distributions

Run \ R'_p cms	0.3-0.5	0.5-0.9	0.9-1.5	1.5-2.0	2.0-3.0	3.0-max
I	14	16	19	16	25	16
II	4	5	6	5	8	5

From these tables, using the values of $\sigma p(1-f)$ it is possible to calculate the number of interactions of the different types taking place. It must be noted that not all of these will be recorded as some may have projected lengths less than 0.3 cms.

Run \ Reaction	(i)	(ii)	(iv)	(vi)
I	142	5	1.25 σ	~ 1
II	45	2	.4 σ	~ 0

From this table it is seen that if n A(n,p) events are identified in run I, the cross-section for their observation is

$$= {}^{n}/1.25 \text{ mb.} \qquad \text{——————(1)}$$

The projected track lengths for the four runs are given in Fig. 9. The solid lines represent the observed results and the dotted lines give the calculated contributions from reaction (i).

A random sample of 55 tracks from run I was analysed using the more accurate method described in Chapter IV. In the following table the projected track lengths so obtained are compared with those obtained for the same sample using the approximate method. The results for the approximate method are marked (a).

Method \ R'_p cms	0.3-0.5	0.5-0.9	0.9-1.5	1.5-2.0	2.0-3.0	3.0-max
(a)	8	13	9	4	4	2
(b)	12	17	7	4	3	2

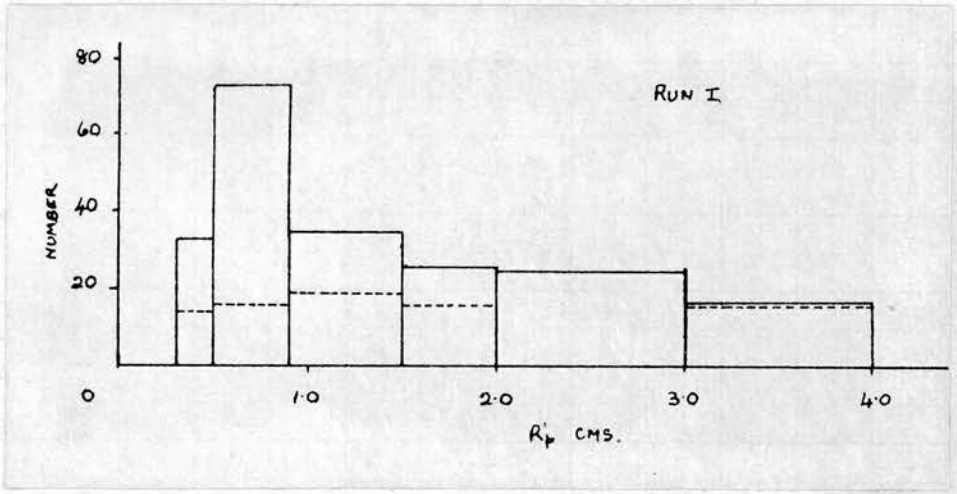
RUN I
NUMBER
80
60
40
20
0
1·0
2·0
3·0
4·0
R'p CMS.

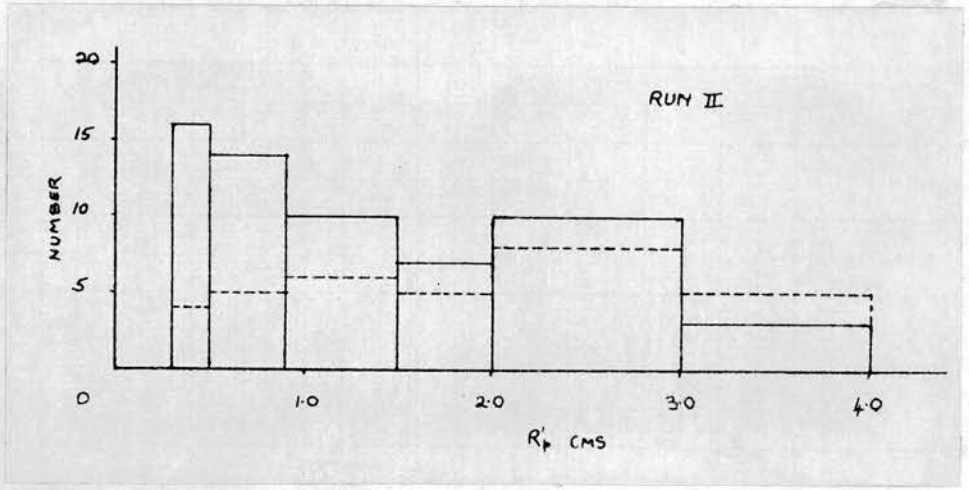
RUN II
NUMBER
20
15
10
5
0
1·0
2·0
3·0
4·0
R'p CMS

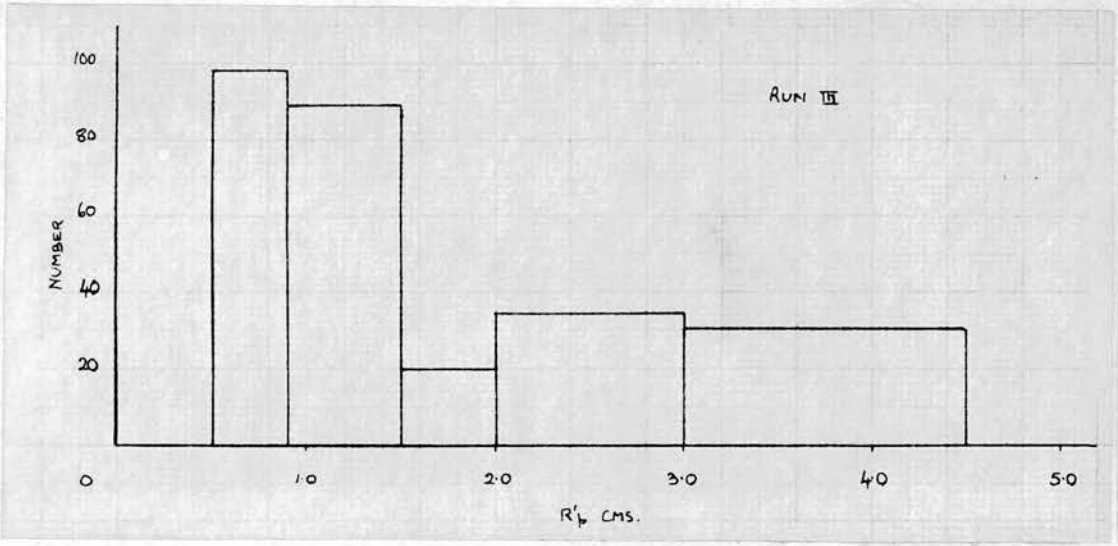
RUN III
NUMBER
100
80
60
40
20
0
1·0
2·0
3·0
4·0
5·0
R'p CMS.

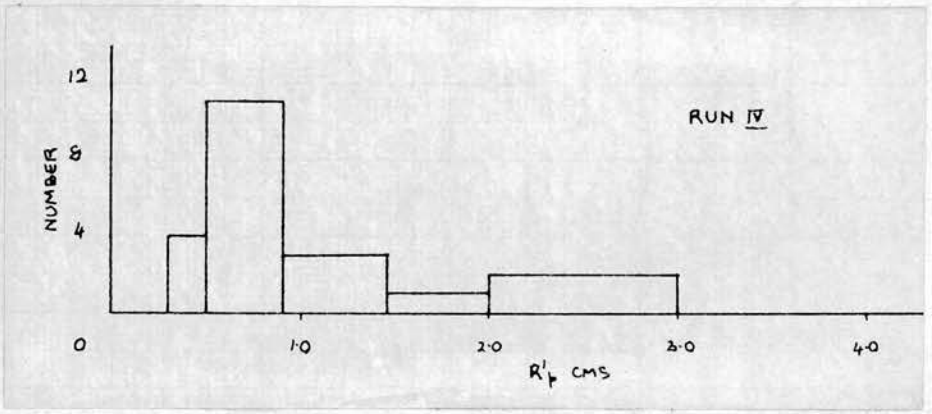
RUN IV
NUMBER
12
8
4
0
1·0
2·0
3·0
4·0
R'p CMS

Fig . 9.

The agreement is seen to be reasonable although there is evidence in case (a) of a flattening of the peak in the range (0.5-0.9)cms, while the total number of tracks recorded with $R_p' \geqslant 0.3$ cms is five less.

The peak is found to be even sharper when the particle ranges are obtained. In Fig. 10 these ranges have been converted into the corresponding proton energies. Five tracks are not shown in Fig. 10 - these have energies greater than 10 Mev. The dotted curve indicates

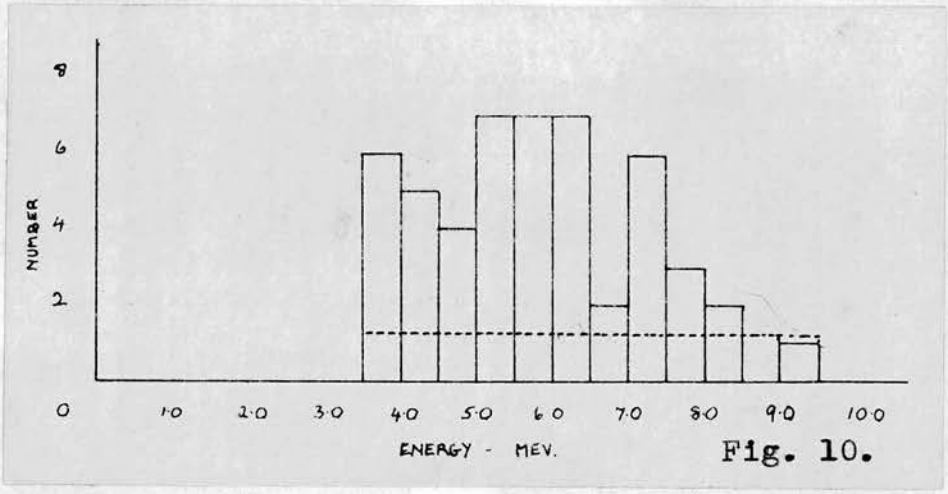

Fig. 10.

the contribution expected from the H(n,p) reaction and is based on the distribution obtained by the approximate method. Some caution should be exercised in the interpretation of Fig. 10 because of the small number of particles involved, but there appears to be a quite definite peak below 7.5 or 8.0 Mev. There is also a possibility of minima in the regions near 6.5 Mev and 4.5 Mev. Below 4.5 Mev the errors in the measurement of the particle ranges become significant and a

contribution might be expected from the A(n,α) reaction. (An α-particle has four times the energy of a proton of the same range).

There is no evidence of contributions in the region of the peak in the projected track length distribution from reactions involving neutrons scattered through angles of the order of 90° at the back of the chamber and producing heavy particle tracks with small projected lengths but large actual lengths. No example was found in the sample of 55 tracks of a track with ΔZ much larger than Δx and Δy.

Some evidence was found of a grouping of the tracks of particles of range greater than 1 cm about a line approximately coincident with the neutron beam direction. This suggests that most of the neutrons entering the chamber had experienced no large angle deflections in the chamber walls and that few neutrons entered the chamber after being scattered by the walls, floor or ceiling.

It has been concluded that the particles in the energy range 4.5 - 8.0 Mev not due to the H(n,p) reaction are due to the A(n,p) reaction. A maximum proton energy of 8.0 Mev would suggest a Q-value for the reaction to the ground state of Cl^{40} of -6.2 Mev corresponding to a maximum energy of the electrons in

the subsequent β-decay of 7.0 Mev. The β-energy spectrum reported by Morinaga has an end-point at 7.5 Mev. The peak in the energy distribution in the region 5.0 - 6.5 Mev might suggest the possibility of one or more states in the Cl^{40} nucleus at an energy 2.0 - 3.5 Mev above the ground state.

It is now possible to interpret the projected track length distributions in more detail. For a proton of energy 8.0 Mev the maximum value of R_p' is 1.4 cms, and in run I, 92 tracks in the range $0.3 \leq R_p' < 1.5$ cms may be allocated to the A(n,p) reaction. No contribution is expected from the A(n,α) reaction in this range, while some events may have been lost because of the approximations upon which the system of observation is based. Substitution of n = 92 in equation (1) of this chapter gives a cross-section of 73 mb.

In run II the distance between the neutron source and the cloud chamber was increased to 4 metres so the solid angle subtended by the chamber at the source was reduced considerably. Under these conditions a greater proportion of scattered neutrons would be expected to enter the chamber. The number of tracks observed in this run was not large but there is some evidence of a decrease in the mean neutron energy in the shift of the position of the distribution maximum.

The peak in the distribution in run IV is apparent although the total number of tracks is small. Few H(n,p) events were expected in this run as the amount of hydrogen present was small. The distribution is consistent with the values of $\sigma p(1-f)$ for this run.

It has not been possible to interpret run III in detail. It seems probable that the reaction $N^{14}(n,p)C^{14}$ leads predominantly to the formation of C^{14} in excited states.

Heavy particle tracks with associated electron track.

Only one event of this type was found in the argon runs. This event is to be seen in Plate 2. The heavy particle track has well defined edges and is unlikely to be a superposition of short electron tracks. The heavy particle range is 1.27 mms corresponding to a proton energy of 2.1 Mev or an α-particle energy of 8.4 Mev. The electron travels a distance 1.3 cms before leaving the chamber so the energy cannot be less than 0.8 Mev. There is some evidence for an increase in multiple scattering with increasing distance from the heavy particle track.

A second (doubtful) event was found in run IV. The end of the electron track furthest from the heavy particle track is very near a cosmic ray track and there is a possibility of the electron being an energetic δ -ray,

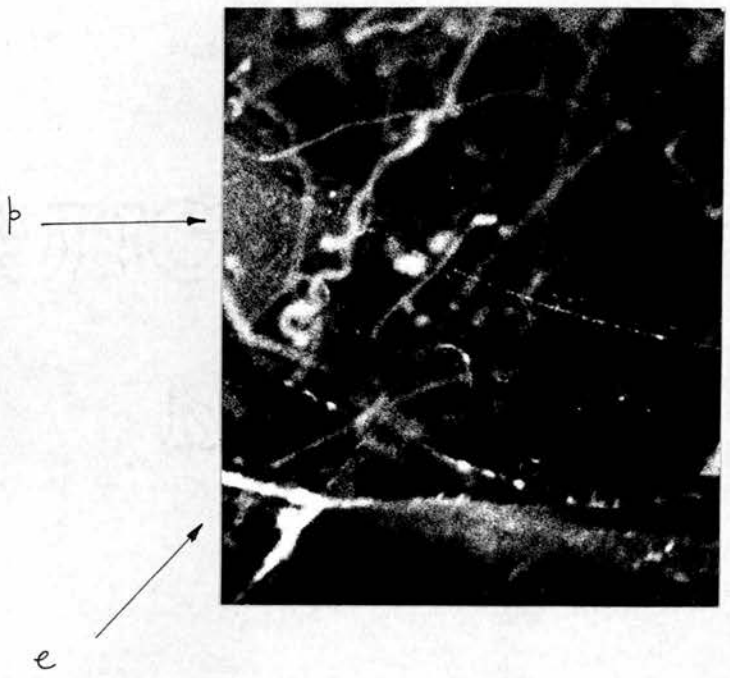

PLATE 2

caused by the cosmic ray particle, stopping in the chamber gas very close to the heavy particle track. The electron track length is 2.2 mms corresponding to an energy of 0.97 Mev. The heavy particle could be a proton of energy 3.1 Mev or an α-particle of 12.4 Mev.

No events were found in run III. It was estimated that there were approximately three times as many heavy particle tracks in the range 0.2 - 0.4 cms in run III as there were in runs I and II, while the total number of electron tracks in the two cases was about the same, so it seems unlikely that the event was due to the chance superposition of a heavy particle track on an electron track.

The event may be an example of the decay from an isomeric state of Cl^{40} but the particle energies are consistent also with its being due to any one of reactions (v), (vi) or (iv). The number of these reactions expected in runs I and II has been calculated using the $pf\sigma$ values for these runs. A cross section of 73 mb has been assumed for reaction (iv).

Reaction	(iv)	(v)	(vi)
Number	.67	.09	.09

If the event is due to the A(n,p) reaction followed

by β-decay from the ground state, the Cl^{40} nucleus must have been formed in an excited state and subsequently decayed by γ -emission to the ground state. A proton energy of 2.1 Mev would suggest a Q-value in the range -11.5 Mev to -12.1 Mev. This would correspond to the formation of the Cl^{40} nucleus in a state with energy 5.3-5.9 Mev above the ground state.

Competition from other reactions can be seen to be considerable, but if this event is an example of β-decay from an isomeric state of Cl^{40} the cross section for the observation of one event in runs I and II assuming f = 1 is 0.61 mb. It must be noted that the efficiency of scanning the photographs for events such as this must be very low because of the shortness of the heavy particle track.

Summary of Results.

(a) The cross-section for the β-decay from an isomeric state of Cl^{40} is not greater than 0.61 mb.
(b) The cross-section for the reaction $A^{40}(n,p)Cl^{40}$ is of the order of 73 mb.
(c) The Q-value for the formation of Cl^{40} in the ground state is of the order of -6.2 Mev.

The cross-sections are for neutrons of energy approximately 14 Mev while the Q-value is calculated for a neutron energy of 14.3 Mev.

REFERENCES : Chapter VII

(1) Ross et al. : Phys. Rev. 85, 11, 1952.

(2) Lillie et al: " " 87, 716, 1952.

(3) Smith et al.: " " 95, 730, 1954.

(4) Morinaga : " " 103, 504, 1956.

(5) Endt et al. : Rev. Mod. Phys. 29, 683, 1957.

(6) Hughes, D.J.: "Neutron Cross-Sections", 1955, p. 85.

CHAPTER VII

INTRODUCTION TO THE μ-MESON EXPERIMENT

The preceding chapters dealt with one method of investigating the β-decay described in Chapter I. The other method outlined in that chapter, that is, the method involving μ-meson absorption in argon, will now be described.

The negative μ-mesons were obtained from the 156 inch synchro-cyclotron of the University of Liverpool.[1] A beam of protons of energy 383 Mev strike a half inch thick target of Beryllium situated inside the cyclotron vacuum chamber. π-mesons are produced by the reaction

$$p + n \longrightarrow p + p + \pi^-$$

Some of the π-mesons decay in the neighbourhood of the target and the beam of particles of momentum 190 Mev/c which is deflected out of the vacuum chamber by the fringing magnetic field of the cyclotron contains μ-mesons resulting from these decays. The particles pass through the field of a focussing magnet and enter a 15 foot long channel through the concrete shielding wall. This acts as a collimator. A magnet placed beyond the collimator deflects the beam through 15°, so removing uncharged particles, and the beam focus is a

few feet in front of the deflecting magnet. The cross-sectional area of the beam at the focus is about 12 square inches and 5-10% of the particles in the beam at this position are negative μ-mesons.

The π-mesons were prevented from entering the cloud chamber by the use of copper absorber. The differential range curve for the beam particles in copper has the

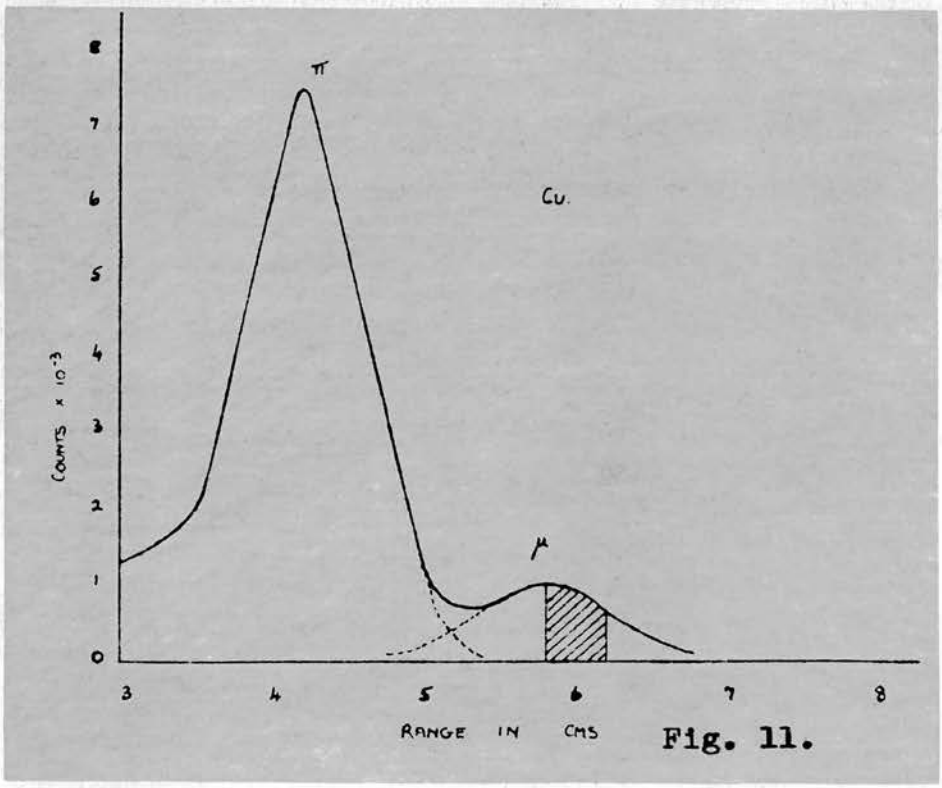

Fig. 11.

form shown in Fig. 11. The main peak with a maximum at 4.2 cms is due to the π-mesons while the small peak at 5.8 cms is due to the μ-mesons. Copper of thickness 5.8 cms was placed in the path of the particle beam and in this way most of the π-mesons were removed.

The beam of μ-mesons entered the chamber at a height of 2' 6" above the floor of the room. The cloud chamber

used was the high-pressure chamber described in Chapter II. The chamber was re-sighted with its axis vertical and the front window facing upwards. The recompression and expansion cylinders, originally vertical, were placed in horizontal positions. With the new lay-out it was possible to reduce the length of the copper tubes connecting the chamber to the cylinders. The expansion and recompression valves were replaced by others of the same design but having all dimensions doubled while the old copper tubing of internal diameter $\frac{1}{2}$" was replaced by $\frac{3}{4}$" tubing. These modifications had the effect of reducing the time taken to expand and recompress the chamber and thus reducing the amount of heat gained by the gas from its surroundings during each cycle. This was of importance during the present experiment as it was essential to run the chamber with as little track distortion as possible.

The copper absorber necessary to stop π-mesons from entering the chamber was contained in the source plug. This consists of a cylindrical brass plug A (Fig. 12) that screwed into the side of the chamber and sealed against the gas pressure by 'O-ring' and 'Bonded' seals S. A brass container B fits into a cylindrical recess in A, and a series of copper cylinders fit into the container. The cylinders were of known lengths varying

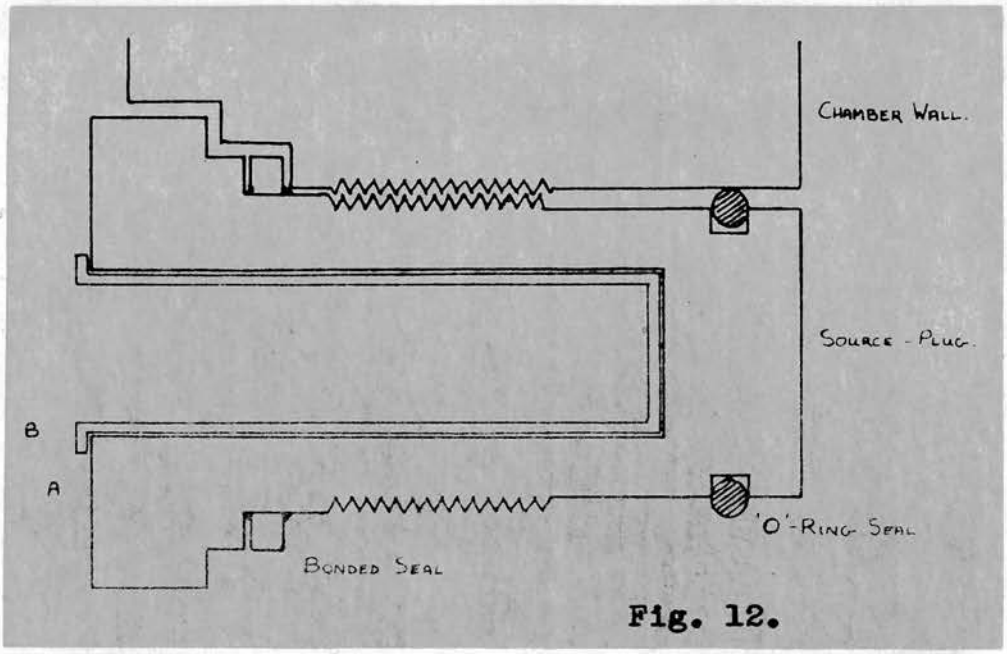

Fig. 12.

from 1 mm to 2 cms, and the number of these in place determines the thickness of absorber through which the beam must pass before entering the chamber gas. The total thickness used, including the end of plug A was 5.8 cms. The chamber wall thickness is approximately 8 cms while the range of 95 Mev/e μ-mesons in steel is 5.5 cms, so few mesons were expected to enter the chamber through the walls. The energy of a μ-meson with a range equal to half the diameter of the chamber is about 10 Mev for a chamber filling of Argon at the pressure used in the experiment. The range of a 10 Mev μ-meson in copper is $\sim$ 0.4 cms, so the fraction of the μ-mesons stopping in the chamber gas is equal approximately to the fraction between 5.8 cms and 6.2 cms in Fig. 11. This fraction is about one quarter.

REFERENCES: Chapter VIII

(1) More: Nature, 175, 1012, 1955.

CHAPTER VIII

NEW ELECTRONIC CIRCUITS

(a) The Cyclotron Circuits

A co-axial cable from the cyclotron control room carried a train of negative 35 volt pulses to the experimental room. If a pulse of the cyclotron beam was required, the appropriate marker pulse was returned to the control room. The pulses arrived at the experimental room at a rate of 110 per second and it was necessary to construct a circuit which would return a known number of these pulses at a pre-arranged time in the cloud chamber cycle. It was also necessary to be able to vary the number of pulses returned and to alter the time in the cycle at which the pulses were returned. The circuit constructed will now be described.

A negative pulse arriving from the cyclotron control room is fed onto the grid of valve V_1 (Fig. 13). V_1 is a pentode amplifier with automatic grid bias. The 120 ohm resistor, r_1, matches the input to the cable from which the pulse is introduced. The output from V_1, a larger positive pulse, is taken from the anode of V_1 and is applied to the first valve V_2 of the Schmitt trigger circuit V_2 - V_3. The potential dividing chain r_6 r_7 r_{10} is so arranged that the grid potential of V_3

is slightly negative with respect to the common cathode. In the quiescent state, v_3 is conducting while the current through r_8 cuts valve v_2 off.* Application of the positive pulse to the grid of v_2 makes it conduct, while the potential at the anode decreases because of the increase of current through r_6. This causes the potential on the grid of v_3 to drop and v_3 cuts off while the cathode follower action of r_8 allows the cathode potential to 'follow' the grid potential of v_2. If the grid and cathode potential fall until they are approximately equal to the grid potential of v_3, v_3 starts to conduct, driving the cathode more positive, and v_2 is cut off once more. The 100 pF condenser in parallel with r_7 allows passage of pulse fronts without their attenuation by stray capacitances. The output, taken from the anode of v_3, is a positive square pulse, the length of which is determined by the shape and magnitude of the input pulse. The height of the output pulse depends only on the value of r_9.

It is possible to cut-off a pentode valve by the application of a negative bias to its suppressor grid. Use is made of this in the gate valve v_4. A bias of -85 volts is applied to the suppressor grid and -6 volts to the control grid and thus the valve cannot pass the positive pulses from the Schmitt circuit unless a large gate pulse is applied to the suppressor grid at

---

* If the control grid of a valve of this type is biassed several volts negative relative to the cathode the valve will not conduct or is 'cut off'.

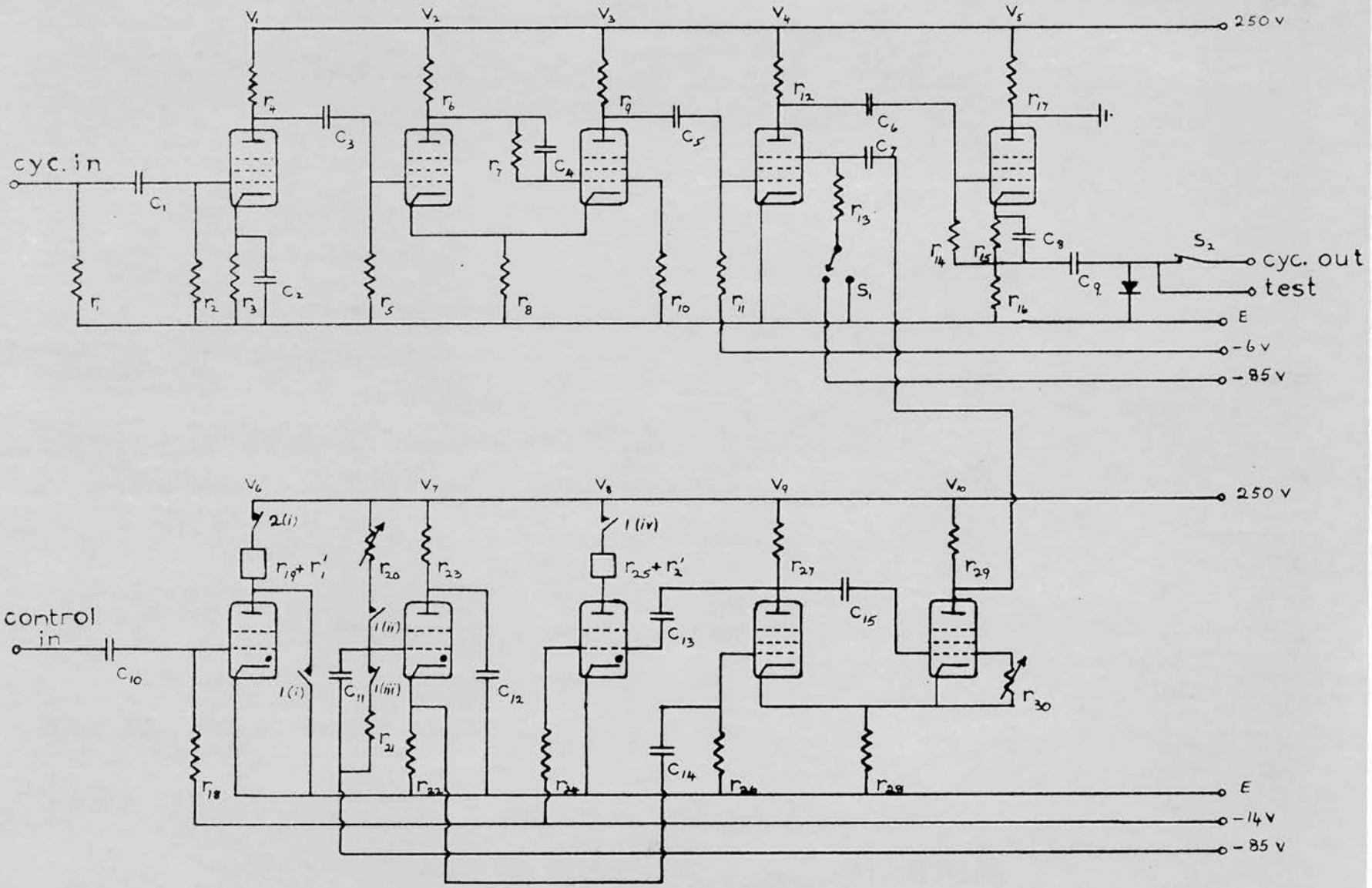
cyc. in
control in
cyc. out
test
250 v
-6 v
-85 v
-14 v
E
V1
V2
V3
V4
V5
V6
V7
V8
V9
V10
r1
r2
r3
r4
r5
r6
r7
r8
r9
r10
r11
r12
r13
r14
r15
r16
r17
r18
r19+r1'
r20
r21
r22
r23
r24
r25+r2'
r26
r27
r28
r29
r30
C1
C2
C3
C4
C5
C6
C7
C8
C9
C10
C11
C12
C13
C14
C15
S1
S2
1(i)
2(i)
1(ii)
1(iii)
1(iv)

Fig. I3.

FIG. 13 COMPONENT VALUES

All resistances are ½W unless otherwise stated.

r_1	120 Ω	r_{16}	33K	c_1	.1 μF
r_2	100 K	r_{17}	5K	c_2	2 μF
r_3	170 Ω	r_{18}	100K	c_3	.1 μF
r_4	5 K	r_{19}	10K	c_4	100 pF
r_5	100 K	r_{20}	500K VAR.	c_5	.01μF
r_6	47 K	r_{21}	22 Ω	c_6	.01μF
r_7	10 K	r_{22}	1.8K	c_7	.1 μF
r_8	47 K	r_{23}	220K	c_8	2 μF
r_9	2.2 K	r_{24}	100K	c_9	.1 μF
r_{10}	5 K	r_{25}	10K	c_{10}	.1 μF
r_{11}	1 M	r_{26}	1 M	c_{11}	2 μF
r_{12}	2.2 K	r_{27}	47K	c_{12}	.5 μF
r_{13}	1 M	r_{28}	680 Ω	c_{13}	100 pF
r_{14}	210 Ω	r_{29}	5.6K	c_{14}	.01 μF
r_{15}	68 Ω	r_{30}	2.2M	c_{15}	.01 μF

r_1' r_2'	P.O. 2K
v_1 - v_5, v_9, v_{10}	EF 91
v_6 - v_8	EN 91

the same time. This gate pulse can be much longer than the Schmitt pulses and its length determines the number of regularly spaced Schmitt pulses that pass through the gate. The gate pulse is obtained as follows.

A positive pulse, supplied by the chamber control circuits is applied to v_6. This valve is a thyratron which is normally cut off by a 14 volt negative bias applied to its control grid. v_6 contains relay coil r_1' in its anode circuit. Application of the positive pulse starts the discharge through v_6 and r_1' is energised. The contacts 1(i) close, extinguishing the discharge through v_6 but allowing r_1' to remain energised. At the same time 1(ii) closes and 1(iii) opens, and c_{11} starts to charge through resistance r_{20}. v_7, a thyratron originally cut off by the -85 volt bias applied through 1(iii), starts to conduct when the condenser has charged to near earth potential. The time interval between the striking of v_6 and that of v_7 depends on the time constant $r_{20}c_{11}$. The output pulse from v_7 is taken from the cathode, and the thyratron discharge is extinguished by means of capacitance c_{12} which discharges through the cathode resistance at such a rate that the voltage across v_7 is insufficient to maintain the discharge.

An output pulse is taken from v_7 to v_9 and v_{10} which form a Kipp Relay. In the quiescent state v_{10} is conducting with its cathode and grid at the same

potential because of the grid leak resistor r_{30}, while v_9 is cut off because the common cathode is positive with respect to the grid. Application of the positive pulse to the grid of v_9 makes v_9 conduct while the resultant large negative pulse at the anode is fed through c_{15} to the grid of v_{10} and v_{10} is cut off. The current drawn by v_9 through the cathode resistor is small and v_9 continues to conduct. Current now flows through r_{27}. to charge c_{15}, the potential of the grid of v_{10} approaching the common cathode potential exponentially with time constant $r_{27}c_{15}$. Eventually v_{10} starts to conduct again and v_9 is cut off by the increase in cathode potential. The negative pulse taken from the anode of v_9 is differentiated by c_{13} and R_{24} resulting in a negative pulse followed by a positive pulse which causes thyratron v_8 to conduct. Relay coil r_2' is energised, contacts 2(i) de-energise r_1' and contacts 1(iv) then de-energise r_2' and extinguish the discharge in v_8.

The output from the anode of v_{10} is a positive square pulse the length of which depends on the length of time for which v_{10} is cut off and thus on the time constant $r_{27}c_{15}$. The shape and size of this pulse are independent of the form of the input pulse to v_9 as long as it is shorter than the output pulse. The input pulse must not be followed by a negative 'overswing' pulse as

this would reset the relay prematurely. This output pulse, the length of which can be varied by the alteration of r_{30}, is the gate pulse which is applied to the suppressor grid of v_4.

The pulse appearing at the anode of v_4 is differentiated by r_{14} and c_6 to give a negative pulse followed by a positive pulse. The negative pulse is fed into the co-axial cable to the cyclotron control room after both pulses have passed through the cathode follower valve v_5 which acts as a low impedance source for the cable transmission. The positive pulse which is not wanted is removed by a Germanium diode connected between the output line and earth.

The instant at which the particle beam enters the chamber is determined by the value of resistance r_{20}. The pulse from the chamber control circuits arrives at the grid of v_6 about 1 second before chamber expansion. The time of beam entry can vary from the instant of closure of the relay contacts of r_1' to a time several seconds later.

A dial was fitted to r_3 and the gate pulse length was found at different settings of the pointer on the dial by counting the number of pulses of known repetition frequency allowed through the gate for each gate pulse applied. The gate pulse length could be varied such that any known number of cyclotron pulses between 1 and 12 could be transmitted.

Switch S_1 enables the gate to remain permanently open in order to test the correct functioning of V_1, V_2, V_3 and V_5, while S_2 was fitted so that the circuit could be disconnected from the cyclotron controls during testing of the circuits or chamber.

(b) The Clearing Field Circuit

Modifications were made to the circuit producing the cloud chamber clearing field, so that the field could be removed more rapidly. The reasons for making the changes are best explained by comparison of the conditions in the neutron and μ-meson experiments.

In the neutron experiment the beam was entering the chamber continuously for one second before the expansion took place. The clearing field was not removed until just before expansion, but since the voltages on the clearing field electrodes were not high ($\pm$ 700 volts), not many of the ions formed by neutron reactions were swept away before the field was removed. A fairly high background of cosmic ray tracks was unavoidable under these conditions.

In the μ-meson experiment however the particles entered the chamber only a fraction of a second before the expansion. In order to decrease the background of cosmic ray tracks a far larger clearing field was used and this was removed immediately before the particle beam

entered the chamber. Thus the faster the field could be removed the longer it could stay on and the less would be the background. It was for this reason that the clearing field circuitry was altered.

The circuit in its new form is illustrated in Fig. 14. 3000 volts A.C. from the high voltage transformer is rectified and the A.C. component is reduced by condensers c_1 and c_2. The voltage v appearing on the transformer side of r_1 is approximately 3,700 volts. Components r_2 and r_3 consist of a chain of seven fixed resistors and one variable resistor connected between the fixed contacts of a single bank rotary switch in such a way that the resistance between the rotating contact and earth could vary continuously between $(7r_2 + r_3)$ and zero.

During the time when the clearing field is applied across the chamber the thyratrons v_1 and v_1' are kept in a non-conducting state by means of a negative bias of their grids with respect to their cathodes, and the contacts 2 and 3 are open. Under these conditions the output voltages taken from the moving contacts of the rotary switches can be varied between $(7r_2 + r_3/r_1 + 7r_2 + r_3)$ xV, and zero.

v_2 is a thyratron which is normally in a non-conducting state. If a positive pulse from the control circuits is applied to the grid, v_2 starts to conduct,

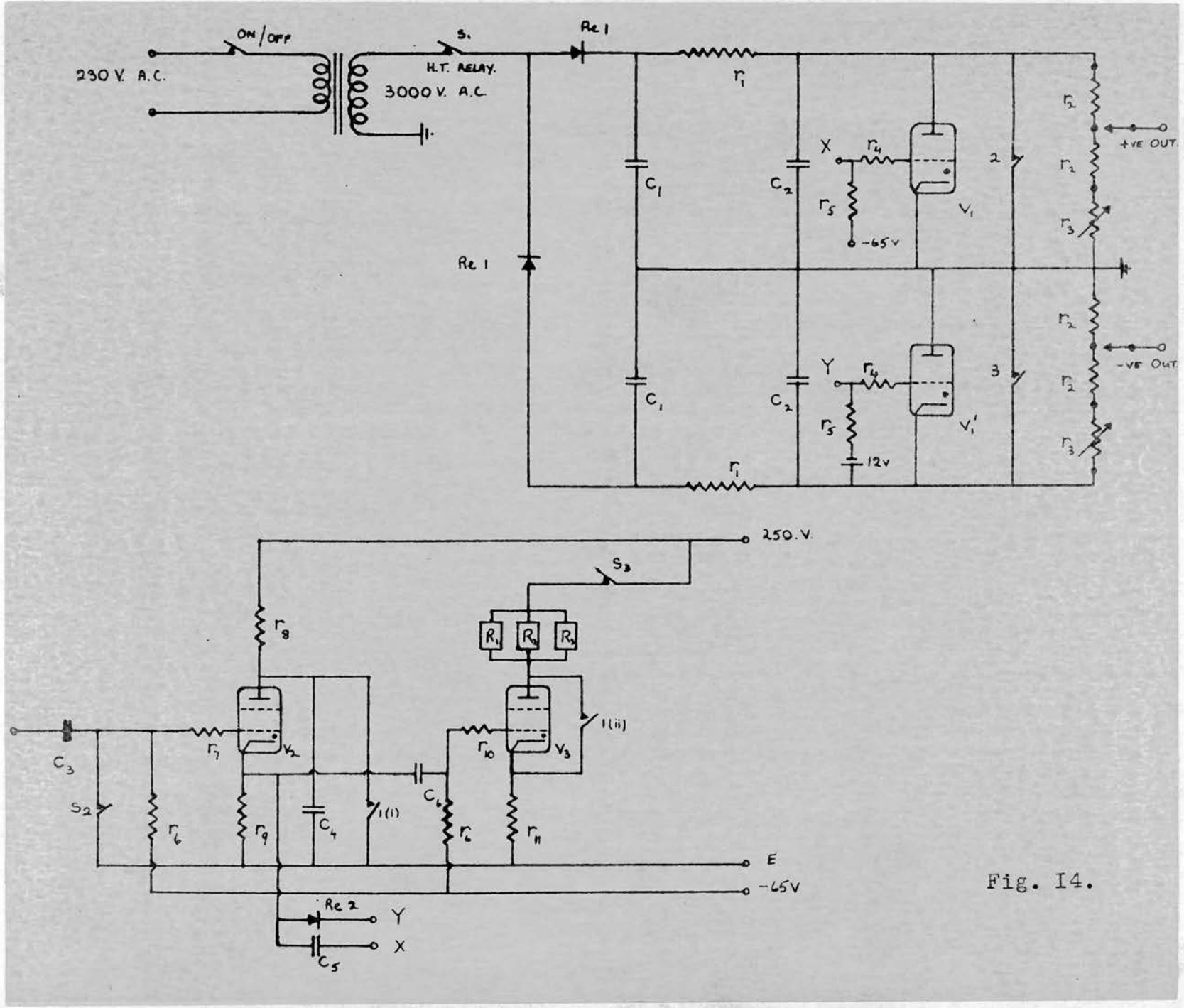
ON/OFF
S1
230 V. A.C.
H.T. RELAY.
3000 V. A.C.
Re 1
Re 1
r1
C1
C2
X
r4
r5
-65 V
V1
2
r2
r2
r3
+VE OUT.
Y
r4
r5
12v
V1'
3
r2
r2
r3
-VE OUT.
250.V.
S3
r8
R1
R2
R3
V2
V3
I(ii)
r7
r10
C3
S2
r6
r9
C4
I(i)
C6
r2
r11
E
-65V
Re 2
Y
X
C5

Fig. I4.

FIG. 14 COMPONENT VALUES

All resistances are ½w unless otherwise stated.

r_1	5 x 47K + 1 x 33K, 8W	r_7	47K
r_2	7 x 220K	r_8	220K
r_3	250K	r_9	2K
r_4	47K	r_{10}	47K
r_5	1 M	r_{11}	2K 8 W.
r_6	100K		

c_1	.1 µF	R_1	P.O. 2K.
c_2	.1 µF	R_2)	Londex 2K
c_3	.01 µF	R_3)	
c_4	.5 µF	Rel	N 388/180
c_5	.01 µF	Ae2	16 TH 160
c_6	.01 µF		

V_1, V_1' XG5 - 500 V_2,V_3 EN.91.

the resultant pulse from the cathode being applied to the grid of v_3 making v_3 conduct. This energises relay coils $R_1 R_2$ and R_3. The discharge in v_2 is extinguished by the quenching capacitance c_4. One pair of contacts of R_1 are connected between the anode and cathode of v_3 and the energising of R_1 causes these to be connected, stopping the conduction through v_3 but allowing the relay coils to remain energised.

v_1 and v_1' are high voltage mercury vapour thyratrons. While conducting, the voltage between the anode and cathode is about 12 volts. Thus if, while the clearing field is on, v_1 and v_1' are made to conduct by application of positive pulses to their grids, the clearing field voltages will rapidly be reduced to a maximum of 12 volts. The necessary pulses are taken from the cathode of v_2. Since the grid of v_1 is only 65 volts negative with respect to earth, the pulse to v_1 can be applied through condenser c_5. In the case of v_1' however the grid, initially at over -2000 volts is brought rapidly to a few volts negative and it is necessary to apply the pulse to v_1' through rectifier Re 2 in order to stop the resultant large positive pulse from being fed back to v_2 and v_3.

The clearing field is finally reduced to zero when the contacts (2) and (3) are closed by the energisation of R_2 and R_3. This action connects the anode to the

cathode on both v_1 and v_1' and thus extinguishes the discharge through these valves. The relay coils R_1 R_2 and R_3 remain energised until contacts S_3, which are part of the chamber control circuitry, are broken. The clearing field is thus re-applied and remains on until another pulse is applied to the grid of v_1.

The circuit used for the neutron experiment consisted of this circuit without v_1 v_1' and v_2 and their associated components. A positive pulse applied to v_3 energised R_1 R_2 and R_3 and the clearing field voltages were removed by contacts 2 and 3. Thus there was a time delay between the application of the initiating pulse and the removal of the clearing field equal to the closing time of 2 and 3.

v_1 and v_1' have directly heated cathodes and since the cathodes are at different potentials, the supplies to the heater filaments are taken from separate tappings on the high voltage transformer. The contacts S_1 of an A.C. relay are placed in the high voltage circuit so that the heaters could be switched on by means of the on/off switch before the large potential differences are applied across v_1 and v_1'.

This circuit could be further refined by biassing the cathode of v_1 12 volts negative and the anode of v_1' 12 volts positive with respect to earth. This would allow the clearing field voltages to fall to zero as

soon as V_1 and V_1' started to conduct. It was not considered necessary to make this modification for the present experiment, but it could be very easily done in the future, as for example in a counter controlled experiment where the positive initiating pulse is supplied by a counter system when a predetermined type of event takes place in the chamber. In this case the track or tracks will not be seen on expansion of the chamber if the field is not removed very rapidly.

CHAPTER IX

ENERGY AND MASS DETERMINATION FROM SCATTERING MEASUREMENTS

A particle passing through a medium suffers deflections in its trajectory due to electro-magnetic interactions with the nuclei of the medium. The scattering observed in a cloud chamber is mainly the result of many small angle deflections but occasionally an interaction takes place that results in a deflection which is sufficiently large to be observed alone.

Suppose that a number of particles of the same mass and momentum pass through thickness t of a given material. The angle ϕ_t between the direction at which a particle enters the material and the direction at which it leaves will be different for each particle, but the mean angle $\bar{\phi}_t$ obtained for a large number of particles is found to be a function of the particle mass and momentum and of the nature and thickness of the scattering material. A value of $\bar{\phi}_t$ can be obtained for a single particle by measuring ϕ_t for successive layers of thickness t of scattering material.

Rutherford (1911) showed that the probability $\omega(\phi)$ of a particle of mass M charge e and velocity βc being scattered by a nucleus of charge ze through angle ϕ was

given by

$$\omega(\phi) = \text{const.} \quad \frac{z^2}{M} \quad \frac{1}{\beta^4 \sin^4 \phi/2} \quad .$$

Rutherford checked this experimentally and found that it was valid at all except very large scattering angles where the scattered particle passes very close to the scattering nucleus and the interaction is not purely electrostatic in nature.

E.J. Williams[1] has given an expression for the mean angle of scattering ϕ_t for a charged particle passing through thickness t of scattering material. In this theory the nuclear charge was assumed to be distributed over a finite volume and on the assumption of the Thomas-Fermi atomic model, Williams took into account the effects of the screening of the Coulomb field by the surrounding electrons. This screening effect is significant at small scattering angles.

For small scattering angles ϕ_t , the angles are found to have a Guassian distribution and are the result of many small deflections. As ϕ_t increases the number of deflections contributing to ϕ_t decreases until at large angles the contributions are almost exclusively from single deflections. The small angle scattering is referred to as 'multiple scattering' and it is in this region that ϕ_t has a Gaussian distribution. The

Williams theory applies to multiple scattering, and large single deflections are eliminated during the experimental determination of ϕ_t .

The method used in the present experiment gave the mean square angle rather than the mean angle and it was necessary to assume a Gaussian distribution of the angles ϕ_t in order to obtain the mean angle from the expression

$$\phi_t = \left(\phi_t^2\right)^{\frac{1}{2}} \times \left(\frac{2}{\pi}\right)^{\frac{1}{2}} \qquad (1)$$

The use of equation (1) necessitates the employment only of those values of ϕ_t which have a Gaussian distribution. In the present experiment, values of ϕ_t greater than $3\phi_t$ were excluded. Employment of this cut-off helps to eliminate single deflections that have not been observed and eliminated previously and it also reduces statistical fluctuations in ϕ_t due to the relatively infrequent occurrence of large angle multiple scattering. A correction factor must be applied to the experimental value of ϕ_t in order to compensate for the application of the cut-off.

The expression given by Williams is for the mean of the projections of the multiple scattering angles onto a plane containing the trajectory of the incident particle. It is valid only when

$$r = {}^{3z}/_{137\,\beta}$$

is much greater or much less than unity. (z is the atomic number of the scattering nuclei.) An expression valid at all values of r has been given by Molière.[2] For incident particles of single charge and of momentum p, Molière gives

$$\phi_t = \frac{2e^2 t^{\frac{1}{2}} z^2 N}{p\beta c} \cdot f(t,z,\beta), \quad \text{where}$$

$$f(t,z,\beta) = 1.45 \times 0.8 \left(\log_e 0.2.\pi.t.z^2 N\left(\frac{\hbar}{me^2}\right)^2 \times \frac{z^2}{137^2.\cdot 3} \Big/ \beta^2 + \frac{z^2}{137^2.\cdot 3}\right)^{\frac{1}{2}} \qquad (2)$$

where t and N are the thickness and number of atoms per cubic centimetre of the scattering material, $\hbar$ is Planck's constant divided by 2π, while m and e are the mass and charge of the electron. c is the velocity of light and ϕ_t is the mean of the projections of the angles of scattering.

The function $f(t,z,\beta)$ is not sensitive to small variations of t and β and for a given scattering medium

$$\phi = c_1/p\beta \qquad (3)$$

for unit t, while

$$\phi_t = c_1'/p\beta\ t^{\frac{1}{2}} \qquad (4)$$

if only small variations of t and β are considered. c_1 and c_1' are constants.

Application

The values of p and β for an electron of energy greater than 3 Mev vary little while the particle traverses the high pressure cloud chamber, and the product pβ and hence the kinetic energy can be obtained as follows. In Fig. 15, Oy is a straight line in the mean direction of the particle track. Equal cells of length $t = y_{n+1} - y_n$ are measured along this line, while TT' is the projection of the particle track onto a plane containing Oy. The coordinates x_n, x_{n+1} of points A_n, A_{n+1} are measured in a coordinate system which is perpendicular to Oy and in the plane of projection. The angle θ_n between the chord $A_n A_{n+1}$ and the direction of Oy is given by

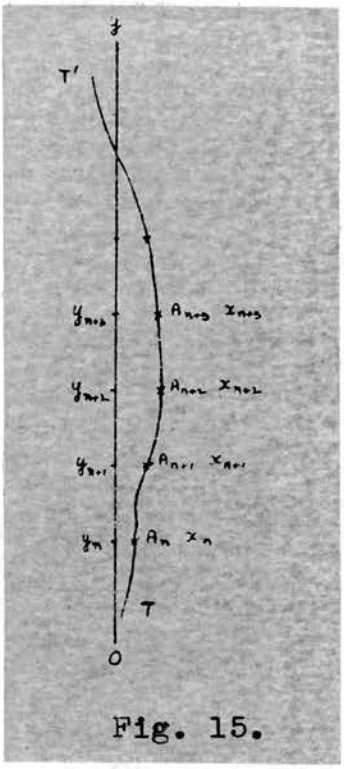

Fig. 15.

$$\tan \theta_n = \theta_n = {}^{x_{n+1} - x_n}/_{t} .$$

The largest angles encountered were of the order of 3° so little error was incurred in assuming $\theta = \tan \theta$.

The angles between successive chords are then

$$\theta_{n+1} - \theta_n = {}^{x_{n+2} - 2x_{n+1} + x_n}/_{t} = {}^{D_n}/_{t}$$

$$\text{i.e.} \quad (\theta_{n+1} - \theta_n)^2 = {}^{D_n^2}/_{t^2} .$$

The mean square angle between successive chords is thus

$$\bar{\theta}^2 = \frac{1}{n} \cdot \frac{1}{t^2} \Sigma_n D_n^2 = \bar{D}_n^2 / t^2 \quad . \qquad \text{(5)}$$

The mean square angle is connected by the following relation to the mean square angle of scattering :

$$\bar{\theta}_t^2 = \frac{2}{3} \bar{\phi}_t^2 \quad , \qquad \text{(6)}$$

the subscripts t being appended to indicate that the angles are those corresponding to a cell length t.

Now from equations (1) and (4)

$$\left(\bar{\phi}_t^2\right)^{\frac{1}{2}} = \left(\frac{\pi}{2}\right)^{\frac{1}{2}} c_1' \, t^{\frac{1}{2}} / p\beta$$

so from equations (5) and (6)

$$\left(\bar{D}_t^2\right)^{\frac{1}{2}} / t = \left(\frac{2}{3}\right)^{\frac{1}{2}} \left(\frac{\pi}{2}\right)^{\frac{1}{2}} c_1' \, t^{\frac{1}{2}} / p\beta$$

$$\text{or} \quad \left(\bar{D}_t^2\right)^{\frac{1}{2}} / t^{3/2} = c_2' / p\beta \qquad \text{(7)}$$

and c_2' can be calculated using equation (2).

Hence measurement of $\bar{D}_t^2$ and substitution of the value in (7) enables p_β to be calculated and if the particle mass is known, it is possible to obtain the kinetic energy.

It is possible to obtain the mass of a particle which stops in the chamber gas, but a somewhat different method must be used. This is because the product $p\beta$ varies rapidly near the end of the particle range. The method used involves the calculation of a series of cell

lengths which vary in such a manner that $\bar{D}_t^2$ of equation (5) remains constant although the product of $p\beta$ is varying. The cell length scheme is calculated as follows.

The kinetic energy E of a particle of mass M, charge Ze and range R is given by

$$E = c_3 Z^{1.16} M^{0.42} R^{0.58} \qquad (8)$$

where c_3 depends only on the medium through which the particle is passing.

For a particle for which $\beta \ll 1$

$p\beta = 2E$ so equation (7) becomes

$$\left(\bar{D}_t^2\right)^{\frac{1}{2}} = c_2' \, t^{3/2}/2E \quad \text{and from (8)}$$

$$\left(\bar{D}_t^2\right)^{\frac{1}{2}} = c_4 Z^{-1.16} M^{-0.42} R^{-0.58} t^{3/2} , \qquad (9)$$

where c_4 is constant while c_3 is constant.

Thus the condition for $\bar{D}_t^2$ to be constant is

$$t^{3/2} \propto Z^{1.16} M^{0.42} R^{0.58} \qquad (10)$$

Using equation (10) a set of values of t are obtained, while $\left(\bar{D}_t^2\right)^{\frac{1}{2}}$ can be found by the method described previously. The value of $\left(\bar{D}_t^2\right)^{\frac{1}{2}}/t^{3/2}$ is now taken for one of the values of t in the series. The corresponding value of R is known and the value of $\left(\bar{D}_t^2\right)^{\frac{1}{2}}/t^{3/2}$ is calculated for a particle of known mass at this range, so if both particles have the same charge,

$$\left(\bar{D}^2_{t_1}\right)^{\frac{1}{2}} / \left(\bar{D}^2_{t_2}\right)^{\frac{1}{2}} = \left(M_1/M_2\right)^{-0.42} \qquad \text{(11)}$$

from equation (9). (The subscripts are used here to identify the two particles).

Elimination of Noise

Associated with every setting of x_n and y_n there is an error of random nature. The mean square value of this error, referred to in the following as noise, is $\bar{\varepsilon}^2$. The observed value of $\hat{D}^2_t$ must now be corrected such that equation (7) becomes

$$\bar{D}^2_t - \bar{\varepsilon}^2 / t^3 = (c_2' / p\beta)^2 \qquad \text{(12)}$$

The signal is $\bar{D}_t^2 - \bar{\varepsilon}^2$, and the signal to noise ratio is thus $\bar{D}_t^2 - \bar{\varepsilon}^2/\bar{\varepsilon}^2$. The signal is proportional to t^3 if the variation of c_2' with t is ignored, while the noise can be assumed independent of t, so the signal to noise ratio can be increased indefinitely by increasing t. As t is increased however, the number of cells is decreased and so is the statistical accuracy of $\bar{D}_t^2$. Biswas et al. have shown[3] that the optimum cell length is that which gives a signal to noise ratio of 5.8. The constant of proportionality in equation (10) is chosen to give this signal to noise ratio, while if the constant cell length method is used the value of t that is employed increases with increase in the value of $p\beta$. In each case the correct signal to noise ratio

is obtained by a method of trial and error.

Now consider the application of equation (12) with two different cell lengths t_1 and t_2. Neglecting the variation of c_2' with t,

$$(c_2'/p\beta)^2 = \frac{(\bar{D}_t^2 - \bar{\varepsilon}^2)_{t=t_1}}{t_1^3} = \frac{(\bar{D}_t^2 - \bar{\varepsilon}^2)_{t=t_2}}{t_2^3}$$

and with $t_2 = t_1/2$

$$(c_2'/p\beta)^2 = \bar{D}_{t_1}^2 - \bar{D}_{t_{1/2}}^2 / 7/8\, t_1^3 \qquad \text{(13)}$$

If the coordinates y_n are now re-defined such that

$$y_{n+1} - y_n = t_{1/2}$$

then for the half cell scheme
$D_n = x_{n+2} - 2x_{n+1} + x_n$, while for the full cell scheme
$D_n = x_{n+4} - 2x_{n+2} + x_n$.

If all values of n are used, the full cell differences are not independent. With $2N + 3$ or $2N + 4$ readings y_n, Biswas et al. quote a standard deviation in $(\bar{D}_{t_1}^2 - \bar{D}_{t_{1/2}}^2)^{\frac{1}{2}}$ of $\pm 0.78/N^{\frac{1}{2}}$. 100% when the signal to noise ratio is 5.8. It was found that the values of c_2' corresponding to $t = t_1$ and $t = t_{1/2}$ differed by only 3% in the present experiment. Since the value of c_2' for $t = t_{1/2}$ only appears in the calculation divided by 8, little error is incurred in taking c_2' constant and using the value corresponding to $t = t_1$. c_2' has also

been assumed constant in calculating the variable cell length scheme. Any significant error in this assumption would result in an observable increase in $\bar{D}_t^2$, with increasing distance from the end of the track $\bar{D}_t^2$, was obtained for the first twenty D-values of four tracks and compared with the value for the second twenty. The former was found to be 4% larger than the latter, the difference being assumed to be a statistical effect.

(b) The Reprojection Technique

The coordinates x_n and y_n were obtained using the method of reprojection. The pressure plate that holds the film against the film gate in the camera was removed and was replaced by a ground glass screen. The developed film was then placed in the camera so as to take up as nearly as possible the position it occupied when the exposure was made. The ground glass screen was then illuminated so that images of objects on the film appeared in space.

The images were located by means of a thin steel needle which was mounted in such a way that it could move in three mutually perpendicular directions, one of which was vertical. The position of the track reprojection was found by adjustment of the steel needle so that it was coincident with corresponding points on each image of the stereoscopic pair at the same time. Each

movement of the needle was provided with a scale with smallest reading 0.001 cms and a scale length of 15 cms. This device has been described by E.J. Williams.(4)

In order to obtain x_n and y_n for a particular track the camera was mounted on a stand and orientated such that the reprojected images were as nearly vertical as possible. The camera was then rotated about a vertical axis until the line joining a point on the track reprojection to the corresponding point on one of the film images was in a plane containing the vertical and one other axis of the measuring instrument (Oy and Oz respectively). If Oz is adjusted each time Oy is altered, the scale readings of Ox and Oy are the required coordinates x_n and y_n.

Several checks were made on this apparatus before it was used - these were as follows:

(i) Trueness of the three perpendicular movements.

Lines were drawn on a piece of film by means of a sharp steel point, and their straightness was checked by means of the Cambridge measuring microscope described in Chapter V. Deviations of up to 0.01 cms from the straight line were observed on the 'reprojected' image when the vertical movement was used. Examination of the surfaces defining the movement by means of the measuring microscope indicated that these were not flat.

Further checks after the surfaces had been remilled were satisfactory.

(ii) Lens distortions

No curvature was detected on the images of straight lines ruled on film, or on the reprojections of photographs of straight lines ruled on a flat ebonite surface.

(iii) Temperature

A rise in temperature of 5°C was found to have no effect on distances measured on the film by means of the measuring microscope.

(iv) Size of the reprojected image

A grating made of ebonite and marked with white lines forming squares of side (2.001 ± 0.001) cms was photographed at various orientations to the camera lens axes. Distances measured on the reprojections were found to be correct to within ± 0.5%.

(v) Position of the film in the gate

Test (iv) results were unaltered when the film was removed from the camera and then replaced. The test was repeated ten times.

(vi) Accuracy of setting the needle on the image

The images of the lines ruled on the film were straight and of constant width 0.02 cms. It was found to be possible to reset the needle on the centre of their images to within ±0.002 cms. Track images in the present experiment were never less than 0.03 cms broad and the width was not constant because of the presence

of low energy delta rays on the tracks. Greater inconsistencies were found in the readings obtained at points on a track where considerable scattering of the particle was in evidence than at other points. In the present experiment a mean of four readings x_n was obtained for each y_n.

The primary application of the theory of scattering in the present experiment was to obtain the energies of electrons associated with the stopped μ-mesons by the constant cell length method. The technique was established by the determination of the mean mass of the stopped μ-mesons using the constant sagitta method. The comparison particle used in equation (11) was the proton. The mass was determined twice for one stopped particle without removal of the film from the camera between determinations in order to observe the effect of inaccuracies in setting the needle on the track image.

The expected distribution of the masses determined by this method has been calculated. Re-writing equation (11),

$$M_\mu = M_p \left(\left(\bar{D}_p^2\right)^{\frac{1}{2}} / \left(\bar{D}_\mu^2\right)^{\frac{1}{2}} \right)^{0.42} \qquad \text{(14)}$$

The experimental values $\left(\bar{D}_\mu^2\right)^{\frac{1}{2}}$ have a Gaussian distribution with standard deviation $\sigma = \left(\bar{D}_\mu^2\right)^{\frac{1}{2}} 0.78 / N^{\frac{1}{2}}$. If $\left(\bar{D}_m^2\right)^{\frac{1}{2}}$ is the value corresponding to $M_\mu = 206.9\, m_e$, then the probability $P\left(\left(\bar{D}_\mu^2\right)^{\frac{1}{2}}\right)$ of observing value $\left(\bar{D}_\mu^2\right)^{\frac{1}{2}}$ is given by

$$P\left(\left(\bar{D}_{\mu}^{2}\right)^{\frac{1}{2}}\right) d\left(\left(\bar{D}_{\mu}^{2}\right)^{\frac{1}{2}}\right) = \frac{1}{(2\pi)^{\frac{1}{2}}} \cdot \frac{1}{\sigma} \cdot e^{-D/2\sigma^{2}} \cdot d\left(\left(\bar{D}_{\mu}^{2}\right)^{\frac{1}{2}}\right)$$

where $$D = \left(\bar{D}_{m}^{2}\right)^{\frac{1}{2}} - \left(\bar{D}_{\mu}^{2}\right)^{\frac{1}{2}} \qquad \text{——————} \quad (15)$$

Substitution for $\left(\bar{D}_{\mu}^{2}\right)^{\frac{1}{2}}$ in terms of M_{μ} and the constants M_{p} and $\left(\bar{D}_{p}^{2}\right)^{\frac{1}{2}}$ gives the probability function for M_{μ}. It is necessary to assume the same value of N for each mass determination.

REFERENCES: Chapter X

(1) Williams E.J. : Proc. Roy. Soc. A169, 531, (1939).

(2) Molière : Zeits. Nat. 3a, 78,(1948).

(3) Biswas et al. : Proc. Ind. Acad. Sc. 38A, 419,(1953).

(4) Williams : Report on Conference on Recent Developments in Cloud Chamber and Associated Techniques, p. 95, London, 1955.

CHAPTER X

μ-MESON CAPTURE AND ABSORPTION

In the experiment performed at Liverpool, negative μ-mesons were stopped in the high pressure cloud chamber. Before describing the experiment it is appropriate to consider in some detail the processes taking place.

A μ-meson entering the chamber with velocity $\beta = 0.36$ will stop after travelling a distance of about 10 cms in the chamber gas. The time taken for the particle to stop is $\sim 2 \times 10^{-9}$ seconds which is small compared with the particle mean lifetime which is $\sim 2 \times 10^{-6}$ seconds, so few of the mesons will decay in flight.

When the meson has a velocity of the same order of magnitude as that of the atomic electrons it becomes captured into an outer Bohr orbit. It then cascades down to an inner orbit, and Fermi and Teller[1] have calculated the time taken for this process to take place. They found that the meson reaches the innermost orbit, that of the 'S state, in a time of the order of 10^{-9} seconds, a time which is also small compared with the mean lifetime for decay. The cascade process is accompanied by the production of Auger electrons and γ-rays. The Auger electrons have been observed in nuclear emulsions[2][3] while γ-ray emission from

mesonic atoms has been studied in some detail in work such as that of Stearnes.(4)

From the 'S orbit the meson either decays or is absorbed by the nucleus. The decay of the negative μ-meson takes place according to the following scheme:

$$\mu^- \longrightarrow e^- + \nu + \bar{\nu} \quad \text{(see Chapter I).}$$

The electron energy may be between zero and a maximum of about 52.5 Mev, and the spectrum shape is sensitive to the nature of the interaction between the particles involved. The interaction Hamiltonian can consist of five relativistically invariant expressions. These are known as the scalar, vector, tensor, pseudo-vector and pseudo-scalar interactions and are denoted by S,V,T,A and P respectively. The Hamiltonian H will consist of a linear combination of some or all of these, thus:

$$H = C_S S + C_V V + C_T T + C_A A + C_p P,$$

and C_x are the coupling constants. Michel(6) has shown that the coupling constants can be obtained by observation of the electron spectrum shape. Recent experimental determinations(7) are consistent with present indications(8) that only V and A interactions are present and that the coupling constants are approximately equal.

The radius of the 'S orbit for a μ-meson is smaller

by a factor m_e/m_μ than that of an electron (m_e and m_μ are the masses of the electron and μ-meson respectively). Considerable overlap of the meson and nuclear wavefunctions takes place because of the smaller orbit radius, and the meson is in a position to interact with a nucleon and be absorbed into the nucleus. The reaction that takes place is

$$\mu^- + p \longrightarrow n + \nu$$

There is a large energy release due to the mass difference between the μ-meson and the neutrino, and much of this energy is removed by the neutrino. Experiments designed to observe the products of the reactions

$$\mu^- + p \longrightarrow p + e^-$$

$$\mu^- + n \longrightarrow n + e^-$$

and $$\mu^- + p \longrightarrow n + \nu$$

have failed to detect the products.[9]

Wheeler[10] has calculated the probability of absorption per second (the 'absorption rate') on the assumption of a point nucleus with probability proportional to the number of protons in the nucleus and to the square of the wave function amplitude in the neighbourhood of the nucleus. This gives a Z^4 variation of absorption probability with Z. The finite nuclear size is allowed for by replacement of Z by Z_{eff} where

$Z_{eff} \leqslant Z$. This effective nuclear charge is obtained by a method of numerical integration, the nucleus being regarded as a uniformly charged sphere. Z_{eff} can be obtained from the following expression:

$$Z_{eff} = Z(1 + (Z/42.0)^{1.47})^{-1/1.47}$$

The Wheeler theory ignores possible spin dependence of the interaction and effects due to the Pauli principle which infers that the neutron must be formed with sufficient energy to reach a vacant neutron state in the product nucleus. The energy required will tend to be greater in the heavier elements because of their neutron excess. Primakoff[11][12] has refined the theory in this respect and gives the following expression for the absorption rate A_{abs}:

$$A_{abs} \cong \Upsilon\left(1 - \frac{A-Z}{ZA} \cdot \delta\right) Z_{eff}^4$$

where A = atomic weight.

The constants Υ and δ can be calculated from known nuclear data and Primakoff gives

$$\Upsilon = 161/\text{sec}, \quad \delta \sim 3.0.$$

The Primakoff theory is not dependent on the type of interaction assumed. Tolhoek[13] has introduced an alternative theory which is sensitive to the form of interaction and suggests a less regular variation of A_{abs} with Z.

Various experiments have been made to determine

absorption rates.[14][15] Sens, in a counter experiment, has obtained results for many elements and using these results finds the best fit to the Primakoff theory when

$$\Upsilon = 188/\text{sec}, \quad \delta = 3.15 .$$

In the table overpage, some of the results of Sens are compared with the predictions of the Primakoff theory using these new constants. Good agreement is obtained with other experimental results. The experimental results are also consistent with Tolhoek's theory with V-A coupling.

The value of Z_{eff} for argon is 15.2 and the calculated absorption rate using the Sens constants is 1.46×10^6/sec.

The nucleus formed by the absorption of a negative μ-meson is usually initially not in a stable state and the absorption process may be accompanied by the emission of heavy particles photons and electrons. The nucleus emits heavy particles until the excess energy is less than the binding energy of the remaining nucleons. It then de-excites by the ejection of photons and electrons. The number of charged heavy particles emitted is expected to be small because of the Coulomb barrier presented to these particles on leaving the nucleus. Morinaga and Fry[16] observed the tracks of 24,000 negative μ-mesons stopping in nuclear emulsions and found only 591 cases

Element	C	$F(KH)_{\frac{1}{2}}$	Al	S	Ca	Cr	Ni	Ag	Tl	u
A_{abs}/sec.x 10^{-5}	0.44	2.54	6.91	13.9	25.5	32.4	60.3	112.5	129.0	109.0
±	0.10	0.22	0.20	0.9	0.5	0.8	1.4	5.0	7.5	5.0
Theory/sec x 10^{-5}	0.44	1.61	6.33	14.4	28.8	35.1	61.7	122	119	93.8

of charged heavy particle emission. Of these, 519 involved the emission of only one particle.

Before predictions can be made about neutron emission it is necessary to make assumptions about the structure of the nucleus. The Fermi gas model[17] in which the nucleus is regarded as an ideal gas of protons and neutrons in equal numbers, and the α-particle model,[18] both appear to be consistent with the few experimental results available.[18][19] Some results are given below for the neutron multiplicity which is the mean number of neutrons emitted per nuclear absorption.

Element \ Reference	18	19
Bi		2.32 ± 0.17
Pb	1.64 ± 0.16	2.14 ± 0.13
Sn		1.54 ± 0.12
Ag	1.60 ± 0.18	
Al		0.95 ± 0.17

Conforto and Sard[20] found that the neutron multiplicity for the lighter elements Ca and Mg was only about 20% of the value for Pb. In order to obtain agreement between the Fermi gas model and experiment it is necessary to assume that the nucleons have only half their normal mass

while taking part in the absorption process[19], a property suggested at an earlier date.[21]

A recent development in the theoretical field is the calculation of the ratio of the absorption rate with no neutron emission leading to the ground state of the product nucleus to the inverse process which is the β-decay of the product nucleus.[22][23][24] The solution of this problem is possible because to a first approximation it is not necessary to assume a nuclear model. The processes involved for absorption in carbon are:

$$\mu^- + C^{12} \longrightarrow B^{12} + \nu$$

$$B^{12} \longrightarrow C^{12} + e^- + \bar{\nu} \ ,$$

and these have been studied using counters[25][26] and a bubble chamber.[27] The results are consistent with a V-A interaction and present experimental knowledge is consistent with this type of interaction in all three processes involving nucleons, electrons, μ-mesons and neutrinos:

$$\mu^- + p \longrightarrow n + \nu \quad \text{(nuclear absorption)}$$

$$n \longrightarrow p + e^- + \bar{\nu} \quad \text{(nuclear decay)}$$

$$\mu^- \longrightarrow e^- + \nu + \bar{\nu} \quad (\mu\text{-meson decay}).$$

(1) Fermi et al. Phys. Rev. 72, 399, 1947.

(2) Cosyns et al. Proc. Phys. Sec. 62A, 801, 1949.

(3) Fry Phys. Rev. 83, 594, 1951

(4) Stearns et al. " " 94, 766, 1954.

(5) de Borde Proc. Phys. Soc. 67A, 57, 1954.

(6) Michel " " " 63A, 514, 1950.

(7) Dudziak et al. Phys. Rev. 114, 336, 1959.

(8) Feynman et al. " " 109, 193, 1958.

(9) Steinberger et al. " " 100, 1490, 1955.

(10) Wheeler Rev. Mod. Phys. 21, 133, 1948.

(11) Primakoff Proc. 5th Annual Conf. (Rochester) 1955, p. 174.

(12) Primakoff Rev. Mod. Phys. 31, 802, 1959.

(13) Tolhoek et al. Nuc. Phys. 3, No. 5, 679, 1957.

(14) Astbury et al. Proc. Phys. Soc. 72, 494, 1958.

(15) Sens Phys. Rev. 113, 679, 1959.

(16) Morinaga et al. Nuovo Cim. 10, 308, 1953.

(17) Tiomno et al. Rev. Mod. Phys. 21, 153, 1949.

(18) Reported Kaplan Phys. Rev. 112, 968, 1958.

(19) Widgoff " " 90, 891, 1953.

(20) Conforto et al. " " 86, 465, 1952.

(21) Bruekner " " 97, 1353.

(22) Fujii et al. Nuovo Cim. 12, 327, 1959.

(23) Wolfenstein " " 13, 319, 1959.

(24) Flamand et al. Phys. Rev. 116, 1591, 1959.

(25) Argo et al. " " 114, 626, 1959.

(26) Burgman et al. " " Letters 1, 469, 1958.

(27) Fetkovich et al. " " 118, 319, 1960.

CHAPTER XI

RESULTS OF THE μ-MESON ABSORPTION EXPERIMENT

Photographs were taken of sets of ten expansions and the film was developed while the succeeding set was being taken. In this way it was possible to check the correct functioning of both the chamber and the synchrotron while the apparatus was in use. The chamber filling was argon at a pressure which varied between 57.5 and 59 atmospheres. Twelve pulses of the particle beam were applied before each expansion. The delay between the last beam pulse and the start of the chamber expansion was estimated to be less than 50 milli-seconds.

The cloud chamber did not function particularly satisfactorily during this experiment and it was found to be necessary to perform a slow cleaning expansion after each set of ten fast expansions in order to reduce the heavy background which was found to build up. It was not possible in the time available to investigate and eliminate this effect.

The photographs were scanned for the following information:

(a) The number N_o of μ-mesons stopping in the chamber and having no associated electron at the end of their range. In counting these it was necessary to exclude

the tracks of stopped protons which exhibit a much smaller degree of multiple scattering and less variation of track thickness with residual range.

(b) The number N_a of μ-mesons stopping in the chamber and causing the ejection of an Auger electron. The maximum Auger electron energy is not greater than 1 Mev so all these tracks are less than 3 cms long.

(c) Stars consisting of one or more secondary particles which are not electrons, and a charged primary.

(d) Stars similar to those of (c) but having no charged primary.

(e) Stopped μ-mesons with an electron of energy greater than 1 Mev at the end of their range. These consisted of N_D μ-e decays and N_e events in which a μ-meson was absorbed by a nucleus which subsequently emitted a decay electron.

No events with both decay electron and Auger electron present were observed so events of types (a), (b) and the nuclear β-decay of (e) were indicative of nuclear absorption of the stopped μ-meson.

The results were as follows:

Event type	(a)	(b)	(c)	(d)	(e)
Number	62	4	2	2	26

The mean angle of scattering varies as the square root of the gas pressure so little error is involved in assuming a constant gas pressure of 58 atmospheres in

expression (2) of Chapter IX, which then becomes

$$\phi_e = \frac{0.206}{p\beta} \cdot t^{\frac{1}{2}} \left(1.45 + 0.80\left(\log e \frac{205.3.t}{\beta^2+0.056}\right)^{\frac{1}{2}}\right) \qquad (1)$$

for argon at a temperature of 20°C.

Part of the cell length scheme used in the determination of the μ-meson is given in the first table on page 99.

The μ-meson mass was obtained using the proton as a comparison particle. A proton of residual range 1.97 cms has a kinetic energy of 10.15 Mev and $p\beta$ = 20.20 Mev/c. The value of t at this residual range is 0.28 cms and the constant c_2' of equation (4) Chapter IX is then 0.7362.

The masses determined for 16 stopped mesons together with their standard deviations are given in the second table on page 99. The method of measurement has been described in Chapter IX.

The mean mass obtained from these 16 tracks was $215 \begin{smallmatrix}+16\\-6\end{smallmatrix} m_e$ while the signal to noise ratio was 7.2.

Most of the tracks studied provided a value of N (see Chapter IX) of the order of 20 and the expected distribution of the observed masses for N = 20 has been calculated. The observed and calculated distributions are shown in Fig. 16. The dotted curve represents the calculated distribution.

The electron energies were obtained using the constant cell-length method. A constant value of $\beta = 1$

Residual Range in cm	.33	.49	.67	.87	1.09	1.32	1.57	1.83	2.11	2.40
t cm	.16	.18	.20	.22	.23	.25	.26	.28	.29	.30

Track Number	1	2	3	4	5	6	7	8
Mass in electron masses	181.1	220.4	412.4	305.4	181.7	166.8	309.1	553.7
S.D.	-28	-33	-49	-67	-28	-24	-46	-76
	+37	+44	+82	+102	+37	+48	+63	+107
Track Number	9	10	11	12	13	14	15	16
Mass in electron masses	334.5	524.4	187.3	234.1	232.2	173.3	182.1	773.4
S.D.	-50	-77	-27	-38	-50	-44	-29	-141
	+72	+100	+41	+49	+90	+68	+46	+227

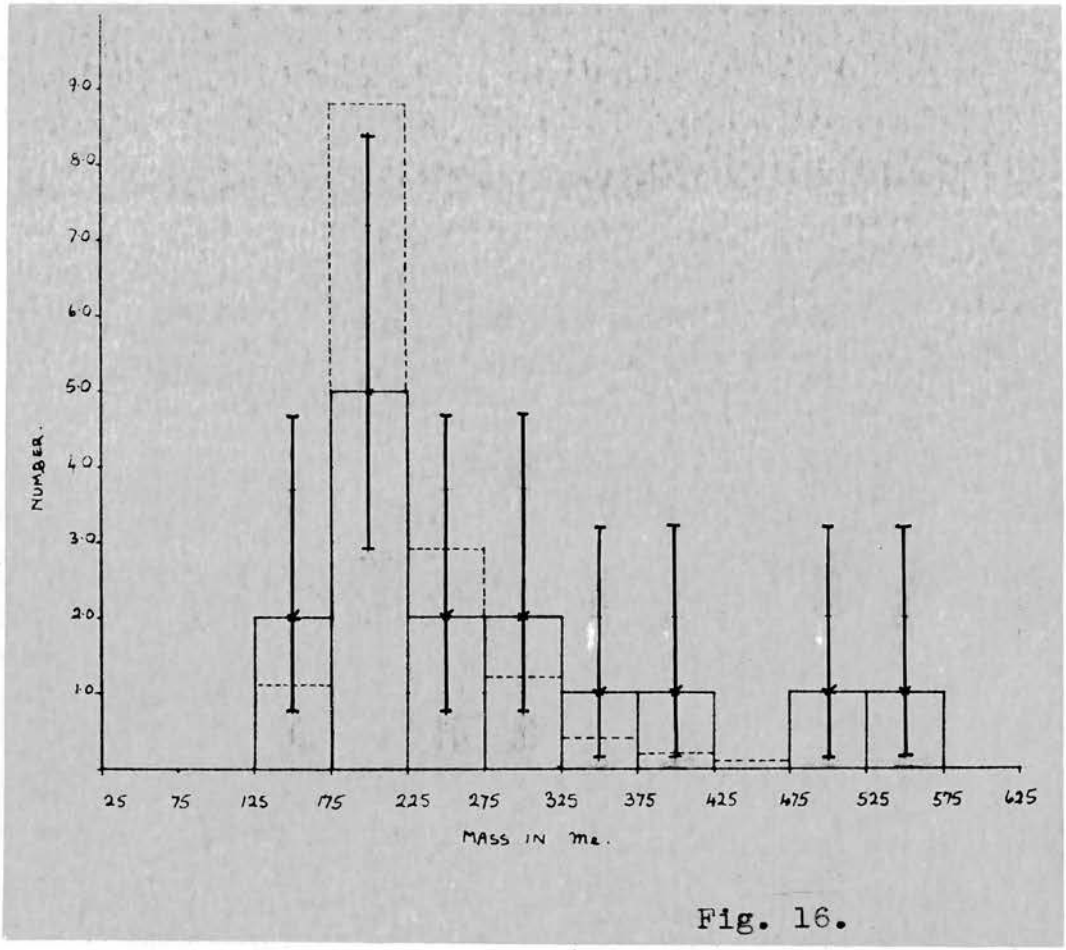

Fig. 16.

was taken inside the log term of equation (1) and in order to obtain the correct magnitude for the signal to noise ratio three different values of t were used, the one chosen for each track depending on the degree of multiple scattering in evidence. The values of t that were used and the corresponding values of c_2' were as follows:

t cms	0.6	0.3	0.2
c_2'	.671	.642	.625

The energies were determined for 24 of the 26 events of type (e). Of the other two, one suffered from

obvious distortion, while the other left the chamber after travelling only 1 cm in the chamber gas. Both events have been omitted from the discussion of the results. In the table overpage the tracks have been arranged in order of energy. The standard deviations quoted in these tables were calculated using the expression of Biswas et al.

It was necessary to correct for the application of the cut-off at $3\bar{D}_t$. The correction factor was determined by plotting the histogram of values of D_t obtained from the stopped μ-meson tracks and superposing a Gaussian curve which extended considerably beyond the cut-off. The histogram was then extended in such a way that it fitted the Gaussian curve and values were obtained for $(\bar{D}_t^2)^{\frac{1}{2}}$ using the full histogram and the histogram ending at $3\bar{D}_t$. The values were found to be in the ratio 1.06 : 1 .

A further set of photographs was taken with the copper absorber thickness reduced from 5.8 cms to 3.8 cms. The photographs were scanned for the following:

(f) The number of stopped mesons with no heavy particle or electron tracks at the end of their range.

(g) The number with one heavy particle track. If the heavy particle stopped in the chamber identification was not difficult. Otherwise identification was by observation of track thickness and very energetic heavy

Track Number	1	2	3	4	5	6	7	8
Energy in Mev	2.5	3.6	3.7	4.7	5.1	7.1	7.4	8.1
S.D.	-0.4	-0.5	-0.7	-1.1	-0.9	-1.3	-1.8	-1.2
	+0.6	+0.6	+1.1	+2.1	+1.2	+2.2	+3.9	+1.5
Track Number	9	10	11	12	13	14	15	16
Energy in Mev	9.8	10.7	15.0	18.1	18.3	21.8	23.3	25.0
S.D.	-1.6	-1.6	-2.6	-4.6	-4.5	-4.3	-6.5	-6.3
	+2.3	+2.1	+4.6	+9.0	+7.9	+7.1	+13.5	+12.6
Track Number	17	18	19	20	21	22	23	24
Energy in Mev	25.3	30.8	30.8	30.9	32.5	32.9	61	120
S.D.	-7.5	-6.3	-5.8	-7.9	-6.3	-8.3	-12	-45
	+15.3	+12.8	+9.1	+15.5	+12.5	+19.2	+23	+130

particles having tracks similar to those of high energy electrons could not be identified.

(h) The number with two heavy particle tracks. In all cases the heavy particles stopped in the chamber.

(i) The number with three heavy particle tracks. These also stopped in the chamber.

(j) The number of events with the appearance of μ -e decays. This group may also contain events of type (g) with a very energetic secondary. In the table of results the numbers followed by a question mark in (g) and (j) could possibly be allocated to the other group. Only those particles that appeared to enter the chamber through the source plug were classified.

The results were as follows:

Type of Event	(f)	(g)	(h)	(i)	(j)
Number observed	16	8+1 ?	5	2	2+1 ?

Discussion of the Results

Examination of the differential range curve for the beam particles in copper (Fig. 11) suggests that with 3.8 cms of copper absorber present, few of the mesons stopping in the chamber will be μ-mesons. If all the events in (f) to (j) are assumed to be due to π-mesons, an upper limit to the number of stopped π-mesons present

in (a) to (e) can be made. Both events of type (c) had only one charged heavy particle secondary, while 9 events of type (g) were observed. This would suggest that a maximum of 4 of the stopped mesons with no heavy particle secondaries in (a), (b) and part of (e) are π-mesons. The three events of (j) would suggest that at the most one of the events classified as a μ - e decay in (e) was a π-meson with a very high energy secondary heavy particle. These figures give the maximum contribution expected from π-mesons. If one of the events in (j) is a genuine μ - e decay approximately 4 of the events in (f) would be expected to be due to μ-mesons and the π-meson contributions to (a), (b) and (e) would be smaller.

The tracks used for the determination of the μ-meson mass were all at least 10 cms long while the π-meson tracks would be expected to be somewhat shorter than those of the μ-mesons, so it is unlikely that a π-meson track has been included in the mass determination. The mean mass obtained is less than one standard deviation from the most recent estimates of the μ-meson mass (206.9 m_e). There is evidence in Fig. 16 of the distribution of the masses of the individual particles being somewhat too broad. The number of particles involved is very small however and it is not possible to draw any conclusions from this observation. It is quite

clear that there is no indication of track distortion of sufficient severity to affect the mass value. This would lead to the observation of a mean mass which was lower than the expected value.

The energies of the electrons have been compared with those obtained by Dudziak et al., who studied the positron energy spectrum resulting from the decay of positive μ-mesons using a magnetic spectrometer. The total number of decay positrons observed was very large and Dudziak's results have been normalised such that there are 15 events with energy greater than 10 Mev. The results are as follows:-

Energy / Experiment	< 10 Mev	10-30 Mev	> 30 Mev
Dudziak	0.2	3.8	11.0
Present	9	8	7

It can be seen that there are rather fewer electrons in the top energy group than expected. The standard deviations quoted for the electrons with energies greater than 20 Mev are very large, while the number of decay events involved in the comparison is small and an explanation of the discrepancy might be found here. Examination of the results in more detail shows that

only two decay electrons were observed to have energies greater than 35 Mev while the energy spectrum should show a peak above this energy.

The apparent shift of the electron energies at the high energy end of the spectrum where the degree of multiple scattering is small has been attributed to track distortion. Distortion of sufficient severity to effect electron energy determination below 10 Mev would have had a considerable effect on the mean mass of the μ-mesons, so track distortion cannot be responsible for the observation of 9 events in this region. The radiation length in argon at 58 atmospheres is $\sim 3.10^3$ cms so the 9 events cannot be μ - e decays in which the electron has lost a large amount of energy by emission of electromagnetic radiation while still close to the point at which the decay took place.

It must thus be assumed that the group of low energy electrons is due to μ-meson absorption. Absorption in the nuclei of the condensant alcohol has a very small probability because of the low values of the absorption rates involved and the small number of nuclei present, so the absorption process must be taking place in argon nuclei. The number of electron emission events allocated to this group is 9, but with the small numbers involved this number may be in error. Thus

$$N_o = 62, \quad N_a = 4, \quad N_e = 9, \quad N_D = 15$$

while the ratio (number of stopped μ-mesons that undergo nuclear absorption) ÷ (number that decay) is $^{75}/_{15}$. With correction for π-meson contamination of the beam, this becomes $^{71}/_{14}$. Assuming a μ-e decay rate of $^{1}/_{2.22 \times 10^{-6}}$ per sec. the absorption rate given by these figures is $(2.3 \pm 0.9)10^{6}$/sec. (The standard deviation quoted contains only statistical uncertainty). The absorption rate calculated for argon using the Primakoff theory is $1.46.10^{6}$/sec.

As was explained in Chapter I the events with low energy electrons must be examples of the β-decay of an isomeric state of an isotope of chlorine. The energy spectrum end-point cannot be given with any certainty but must be greater than 7 Mev.

No events similar to these β-decays were found in the photographs containing a large proportion of stopped π-mesons, so it can be stated with some certainty that the 9 events are not examples of β-decay following π-meson absorption.

The interaction taking place when a negative π-meson is absorbed is:

$$\pi^{-} + p \longrightarrow n.$$

There is thus no light particle formed which can remove a large fraction of the excess energy as there is in μ-meson absorption and it is extremely unlikely that

the π-meson absorption process can take place without the emission of at least one heavy particle. It would thus not be possible to form Cl^{40} by means of the absorption in A^{40} of negative π-mesons, and it might be possible to use this to indicate whether the isomeric state from which the β-decay is observed is in Cl^{40}. No further identification of the active nucleus is possible by means of meson absorption in argon until further details become available of neutron emission during the absorption process.

Photographs are given of a μ - e decay with electron energy (as determined by the measurement of multiple scattering) 25.0 Mev, a β-decay event with electron energy 3.6 Mev and 1-and 2-prong stars resulting from the nuclear absorption of negative π-mesons. These are shown in Plates 3, 4 and 5 respectively.

Summary of Results

(a) The existence of a previously unobserved β-decay in an isotope of chlorine formed by the absorption of negative μ-mesons is confirmed.

(b) The β-decay energy spectrum has an end-point at or above 7 Mev.

(c) There is at least a 50% probability that nuclear absorption of negative π-mesons in argon will be followed by charged heavy particle emission.

(d) The absorption rate for negative μ-mesons in argon is $\sim 2.3 \cdot 10^6$/sec.

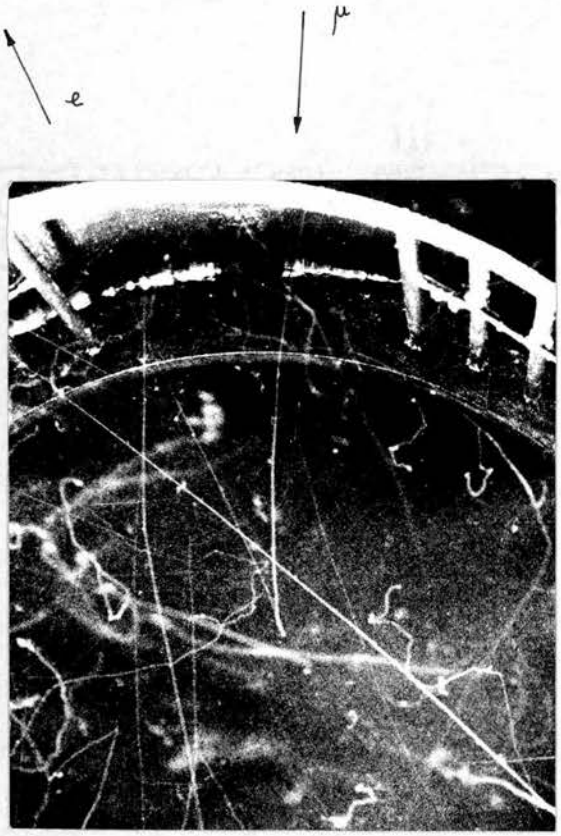

PLATE 3

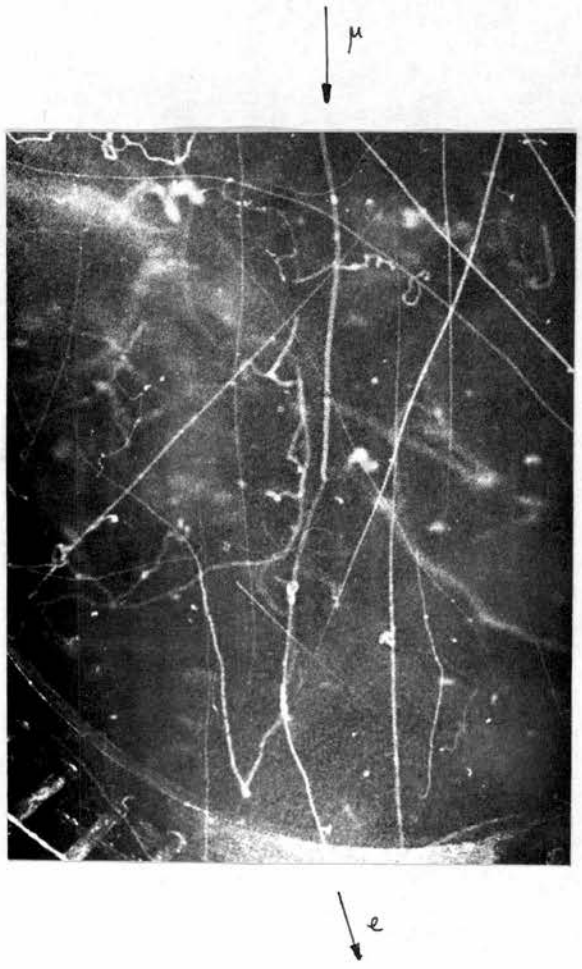

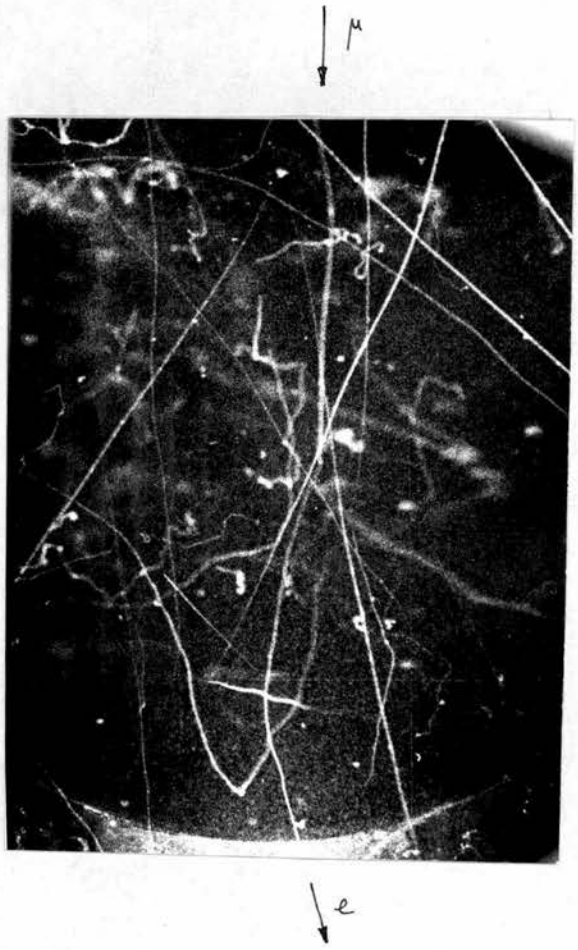

PLATE 4

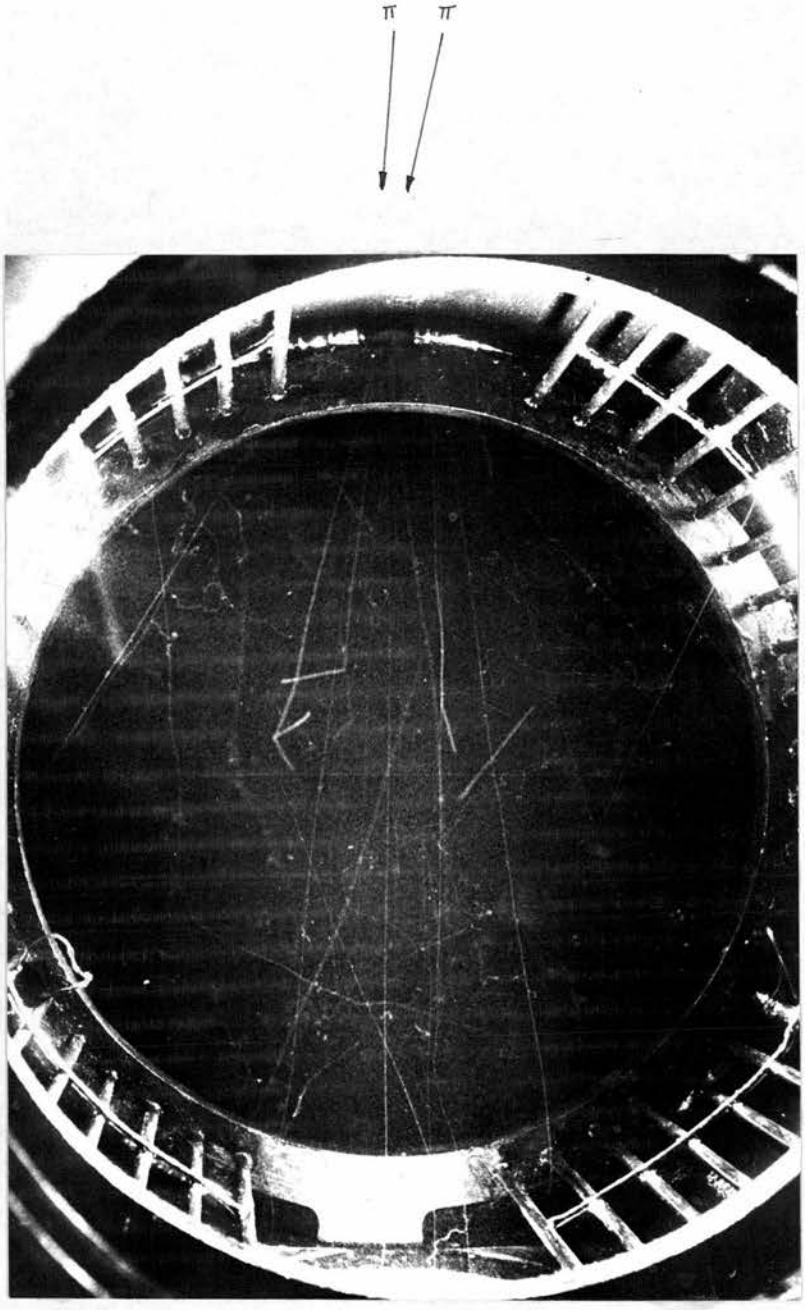

PLATE 5.

CHAPTER XII

CONCLUSIONS

The two experiments described in this text indicate that there exists a previously un-confirmed β-decay of one of the isotopes of chlorine. Observation of the decay electron tracks in the two experiments indicates that the delay between formation of the nucleus and emission of the β-particle is never greater than 200 ms and the decay half-life must be of this order of magnitude or less. The nuclear β-decay events in the μ-meson absorption experiment are small in number but they indicate that the end-point of the energy spectrum is likely to be at least 7 Mev and might be even higher.

The present known β-decay half-lives for Cl^{40}, Cl^{39} and Cl^{38} are 1.4 m, 55 m and 37 m respectively, so it must be assumed that the β-decay takes place from an isomeric state of a chlorine nucleus, but owing to the possibility of the single event in the A(n,p) experiment being due to a competing reaction it has not been possible to identify the isotope containing the isomeric state. Accordingly a nuclear level scheme will be given for several isotopes of chlorine in an attempt to accomodate an isomeric state in each isotope. It is not possible to give a unique scheme for each isotope.

Before the schemes can be outlined it is necessary to discuss briefly some of the properties of the ground and excited states of nuclei. These properties are as follows:

(a) Parity. In quantum theory the state of a system is described by a Schrödinger wave function $\psi(r_1 r_2 \ldots r_n)$ where $r_1 \ldots . r_n$ are the coordinates of the n particles in the state. The function $\psi(-r_1 - r_2 \ldots . -r_n)$ must characterise the state also and the two functions must be identical except for a constant factor c where $c^2 = 1$. Thus

$$\psi(-r_1 -r_2 \ldots . -r_n) = c\psi(r_1 r_2 \ldots . r_n)$$

If c = +1 the state is said to have even parity (designated "+"), while if c = -1 it has odd parity ("-").

(b) Angular Momentum. This contains contributions from the orbital motion of the particles and from their intrinsic angular momentum. It is quantised and the quantum number is J.

(c) Isobaric spin. A quantum number T can be given to each state if the specifically nuclear forces between nucleons are assumed to be charge independent. The third component T_3 of T is given by

$$T_3 = \tfrac{1}{2}(N - Z)$$

and it is found that for the ground state of a nucleus T is usually equal to T_3 . (N = number of neutrons and Z = number of protons). T is only a good quantum number while the electric interactions between protons are small enough to be treated as perturbations. This is so for light nuclei.

There is no simple relationship between half-life τ and end-point energy E_β in β-decay. It is possible to derive a function $f(E_\beta, Z)$ such that the product $f\tau$ can be predicted if the changes in J and in parity of a β-transition are known. Nuclear β-decays are classified as 'allowed' '1st forbidden' and '2nd forbidden' if they have values of $\log_{10}(f\tau)$ in the ranges 3-5, ~7 and ~10 respectively. The selection rules are as follows.

Transition	Parity Change	|J|	$\log_{10}f$
Allowed	no	0,1	3.5
1st forbidden	yes	0,1,2	~ 7
2nd forbidden	no	2,3	~ 10

Function f is tabulated in such publications as "Beta and Gamma-Ray Spectroscopy", Ed. Siegbahn, N. Holland, 1955.

The values of $\log_{10}(f\tau)$ are for τ in seconds.

The selection rules for γ-transitions between two states of a nucleus depend on the multipolarity of the γ-radiation and on whether the radiation is 'magnetic' or 'electric'. The terminology used is as follows - electric 2^L-pole radiation is denoted EL while magnetic 2^L-pole radiation is ML. The radiation is that emitted by the classical electric or magnetic 2^L-pole. The selection rules result from application of the laws of conservation of parity and angular momentum to the system consisting of nucleus and γ-ray. The rules are:

Transition	Parity Change	$\lvert\Delta J\rvert$ *
EL	$(-1)^L$	$\leq L$
ML	$(-1)^{L-1}$	$\leq L$

where there is no parity change if $(-1)^L = +1$.

* Strictly, if J_i and J_f are the values of the initial and final state spins

$$|J_i - J_f| \leq L \leq J_i + J_f .$$

Gamma-emission is forbidden if $|\Delta T| > 1$. The lowest multipole order consistent with $|\Delta J|$ is normally the one observed but there may be a small admixture of higher orders present.

For a given γ -ray energy the transition probability decreases with increasing multipolarity, while for a given multipolarity the probability increases very rapidly with the energy. Approximate values of this probability for a given atomic number, γ -energy and type of transition can be obtained in tabular form.

It is now necessary to construct a nuclear level scheme which would allow the β-decay from an excited state to have a decay half-life of the same order of magnitude as that for the decay by γ-emission to the ground state. With $E_\beta \sim 7$ Mev, $\tau \sim 0.2$ seconds and $z \sim 20$, reference to the tables of $\log_{10} f$ shows that the β-decay is an allowed transition. The lowest value of E_β likely (i.e. that giving $\log_{10}(f\tau) \sim 3$) is $E_\beta \sim 5$ Mev. It is noted that for an allowed transition there is no change of parity, while $|\Delta J| = 0$ or 1.

Three chlorine isotopes have been considered - Cl^{40}, Cl^{39} and Cl^{38}. Cl^{37} is stable, while the formation of Cl^{36} by negative μ-meson absorption would require the ejection of four neutrons which is not likely to happen often. In the three cases considered, the most favourable scheme is that in which the β-decay takes place to the ground state. The decay schemes are shown in Fig. 17 where previously established values of J, parity and energy above the ground state of the daughter nucleus are given. Other β-decay modes are not shown.

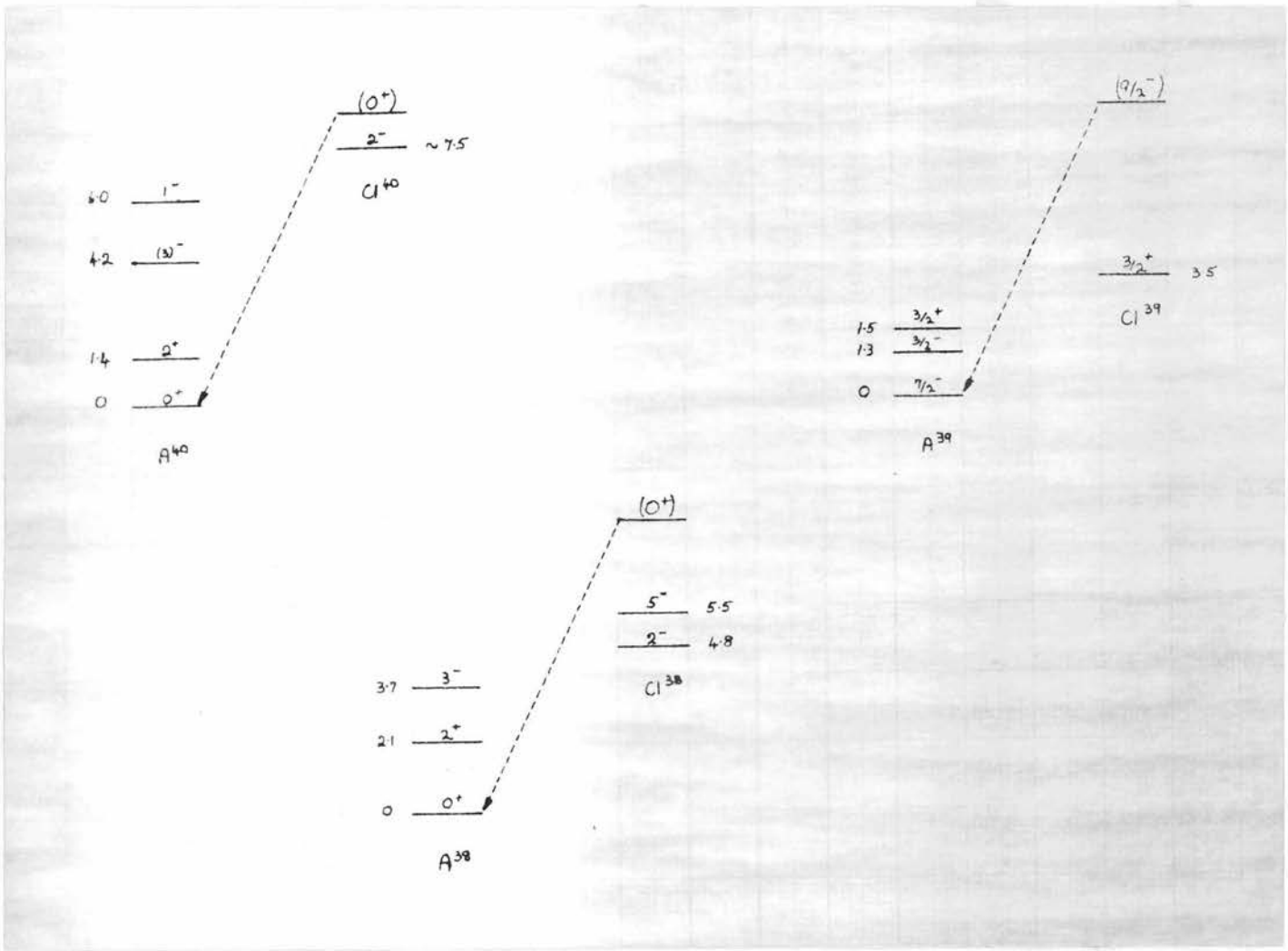
(0+)
2-
~7.5
Cl40
6.0
1-
4.2
(3)-
1.4
2+
0
0+
A40
(0+)
5-
5.5
2-
4.8
Cl38
3.7
3-
2.1
2+
0
0+
A38
(9/2-)
3/2+
3.5
Cl39
1.5
3/2+
1.3
3/2-
0
7/2-
A39

Fig. 17.

In the Cl^{40} decay scheme[1] the isomeric state is 0^+ so the γ-transition to the ground state is M2, and in order to give the required decay half-life, the γ-transition energy must be less than 16 keV. The corresponding E_β would then be $\sim$ 7.5 Mev.

The nuclear level scheme for Cl^{39} [2] indicates an E3 γ-transition and the γ-energy cannot be greater than 100 keV, corresponding to a value of $E_\beta \sim 3.6$ Mev. The $f\gamma$ value for the β-transition is scarcely compatible with those expected for 'allowed' transitions while the results of the μ-meson absorption experiment suggest that in fact E_β is several Mev greater than this.

The Cl^{38} scheme[3] is similar to that for Cl^{40} and the γ-ray energy of the M_2 transition must be less than 16 keV. This would place the isomeric state between the states with energy 4.8 Mev and 5.5 Mev and would suggest $E_\beta \sim 4.8$ Mev. This might just be possible when the magnitude of the standard deviations on the energies of the decay electrons in the μ-meson experiment are considered.

So far the isobaric spin selection rule has not been considered. In all three decay schemes the value of E_β could be larger if the γ-emission was forbidden by this rule. The values of T for the ground states of Cl^{40}, Cl^{39} and Cl^{38} are likely to be 2, 3/2 and 1

respectively so if the isomeric state was the first excited state and it had a value of T differing by 2 or more from these values the γ -transition would be forbidden.

It is unlikely that the isomeric state is in Cl^{39}. The scheme for Cl^{40} fits the experimental results of the μ-meson absorption experiment, but if the isomeric state is in this isotope it is difficult to explain why the cross section for the A(n,p) reaction leading to this state is so small compared with the cross section observed for the formation of the other states of Cl^{40}. Inhibition of deuteron reactions leading to the formation of certain states due to isobaric spin selection rules has been observed[4] but no such effect is expected or observed in (n,p) reactions.

An isomeric state in Cl^{38} is consistent with the experimental evidence. From the small amount of experimental information available it seems likely that approximately one quarter of the μ-meson absorptions in A^{40} will produce Cl^{38} and a similar fraction will produce Cl^{40}. With a total of 75 absorption events in the μ-meson experiment it would be expected that about 19 Cl^{38} nuclei and 19 Cl^{40} nuclei would be formed, mainly in highly excited states. In either case if the probabilities of β-decay and γ -emission from the isomeric state are assumed to be equal, a maximum of 10

β-decay events would be expected, while a possible 9 were observed.

Apart from the experiment involving negative π-meson absorption in argon that was discussed in the last chapter, it might be possible to identify the isotope of chlorine by repeating the neutron experiment in the absence of atmospheric oxygen and using a larger neutron flux. Heavy particle range measurement could be used to discriminate between $A^{40}(n,\alpha)S^{37}$ events and $A^{40}(n,p)Cl^{40}$ events, but the latter might be confused with $A^{40}(n,t)Cl^{38}$ events if the isomeric state is in Cl^{38}. Counter experiments involving the study of the reactions $Cl^{37}(d,p)Cl^{38}$ and $Cl^{37}(n,\gamma)Cl^{38}$ might aid identification while an accurate determination of E_β would help interpretation.

REFERENCES: Chapter XII

(1) Morinaga: Phys. Rev. 103, 504, 1956.

(2) New Nuclear Data 1957, United States Atomic Energy Commission.

(3) Paris et al.: Phys. Rev. 100, 1317, 1955.
Kraushaar et al. : Phys. Rev. 95, 456, 1954.

(4) Adair : Phys. Rev. 87, 1014, 1952.

APPENDIX I

Development of the Fast Recompression Technique

Dr. G.R. Evans and Dr. R.A. Donald of this department have found it possible to run the cloud chamber with fillings of argon or nitrogen at 60 atmospheres pressure with a re-cycling time of 2 minutes if fast recompression was used. This cycle only involves a fast expansion followed 500 m.sec. later by an equally fast recompression - no slow cleaning expansion was required and, in fact, any attempt to include one in the cycle resulted in an increase in the necessary re-cycling time to 15 minutes. This long waiting period was necessary because even the slowest cleaning expansions caused a temperature gradient to be set up across the chamber from top to bottom. This gradient disappeared only very slowly and if the chamber was run on a 2 minute cycle with a slow expansion included in the cycle it was found that after a few expansions had been made tracks were only observed in the lower half of the chamber while the general background of drops increased to an impossibly high degree.

When the fast recompression cycle without a cleaning expansion was first applied to the chamber containing 60 atmospheres of hydrogen these same symptoms developed and it was assumed that in some way similar conditions

were being produced in both cases despite the lack of cleaning expansion in the case of hydrogen.

With argon and nitrogen fillings it was assumed that the effects were due to the heat exchanges taking place between the gas and the chamber walls. In the slow cleaning expansion the time taken may be several seconds as the expansion itself takes some time and a further delay is necessary to allow the drops time to grow and to fall to the foot of the chamber under gravity. At the end of this process the average gas temperature will be close to room temperature and when the gas is recompressed it will rise 10-20^{o}C above this temperature. At this stage heat is given back to the chamber walls and the heat exchange leads to turbulence in the gas and to the establishment of a temperature gradient. The turbulence dies away fairly rapidly and the gas is left in a more stable state so the temperature gradient disappears only very slowly.

These effects are exaggerated when the drops of alcohol are allowed to fall to the foot of the chamber, as this region will be cooled by the subsequent re-evaporation of the alcohol.

It was noted that drop formation in hydrogen was more rapid than in the other gases. This is because the diffusion of alcohol vapour through hydrogen is more

rapid than it is through nitrogen and argon, while the thermal conductivity of hydrogen is higher, and the rate of drop growth depends on the rate at which alcohol arrives at the drop and on the rate at which the heat resulting from the condensation of the alcohol on the drop is conducted away. Because of this more rapid drop growth most of the drops fall to the foot of the chamber before recompression takes place if the cycle that was successful for argon and nitrogen is applied to hydrogen.

It was also noticed that when a period of several seconds was allowed to elapse between expansion and recompression, a dense cloud of drops rose from a glass window situated near the lowest part of the chamber. It was assumed that this cloud was due to the establishment of a cold region near the glass so that when the chamber was expanded the gas in this region was over-expanded and the dense cloud was produced.

It was reasonable to assume therefore that if the fall-out of the alcohol drops could be prevented the performance of the chamber with a hydrogen filling would be satisfactory. The period between the end of the expansion and the beginning of the recompression was reduced until the alcohol drops, while allowed time to grow large enough for photography, were re-evaporated in situ by the fast recompression. Under these conditions the chamber worked well and the limitation on

the re-cycling time was set only by the time it took to re-set the pressures in the expansion and recompression cylinders.

In an effort to make the system even more efficient larger expansion and recompression valves were fitted (see Chapter VII). The new system was used during the experiment performed at Liverpool, but was not entirely satisfactory. This is thought to be due to the re-orientation of the chamber with axis vertical so that there is a large area of poorly conducting glass at the top of the chamber which will tend to slow down the removal of temperature gradients in the gas. Also the gas which lies between the perforated plate and the diaphragm will become hotter than the rest of the gas before recompression takes place and will be pushed up through the plate by the recompression causing turbulence and temperature upset.

The cloud chamber has now been re-mounted with axis horizontal, but has not yet been tested.

APPENDIX II

Electric Discharges in the High Pressure Chamber.

During the operation of the high pressure cloud chamber with an argon filling, electric discharges were observed to take place between the clearing field electrodes. These took the form of intense columns of ions which were observed when an expansion was made. A certain amount of experimental work was performed to study these discharges as it was found that the chamber would not work satisfactorily when they were present. In plate 6 the multiple discharge is from the end of a piece of cotton saturated with alcohol and attached to the electrode after the removal of an insulating layer of paint from it. No such discharge is in evidence from the piece of cotton to be seen to the left of the first piece. In this second case the paint was not removed. The single discharge is from a brass point soldered onto the electrode. The multiple discharges appear to be associated with the ends of individual strands of cotton.

Other observations made were:

(a) The ions appear to be formed in the vicinity of the cotton and brass 'points' and to drift across the chamber under the influence of the clearing field without observable ion multiplication.

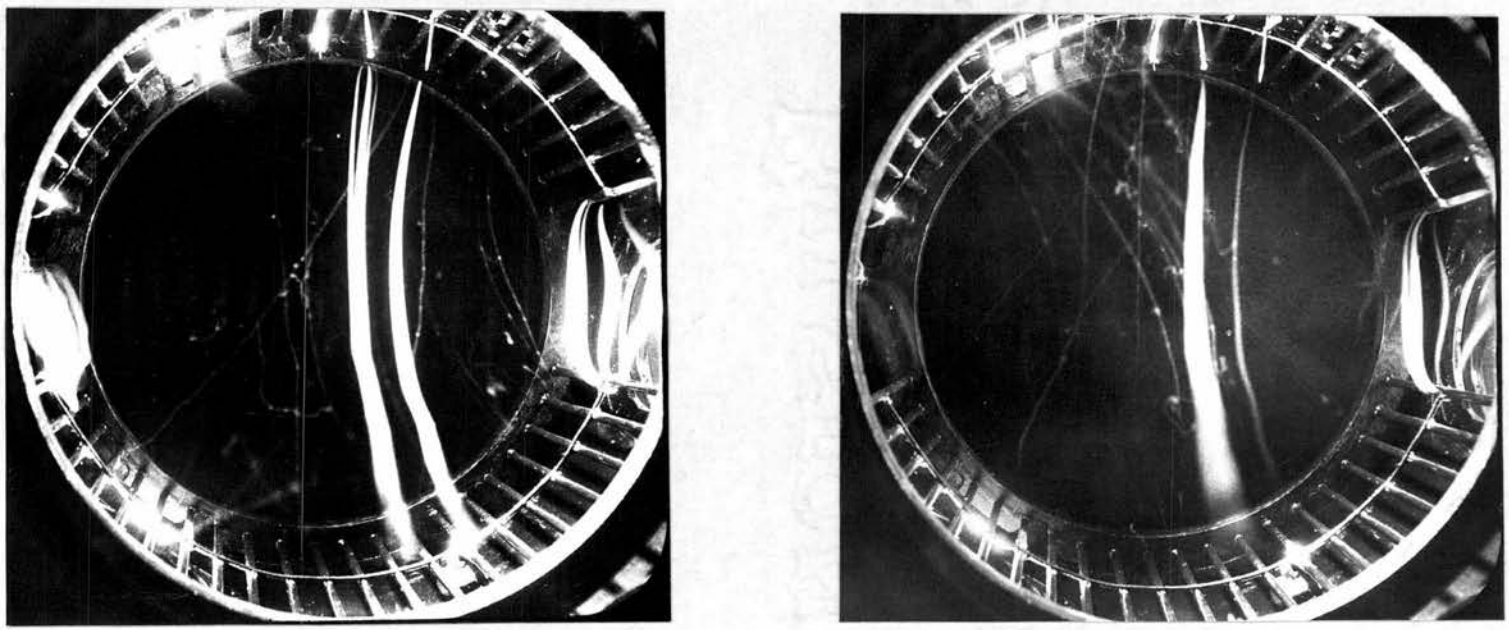

(a) (b)

PLATE 6.

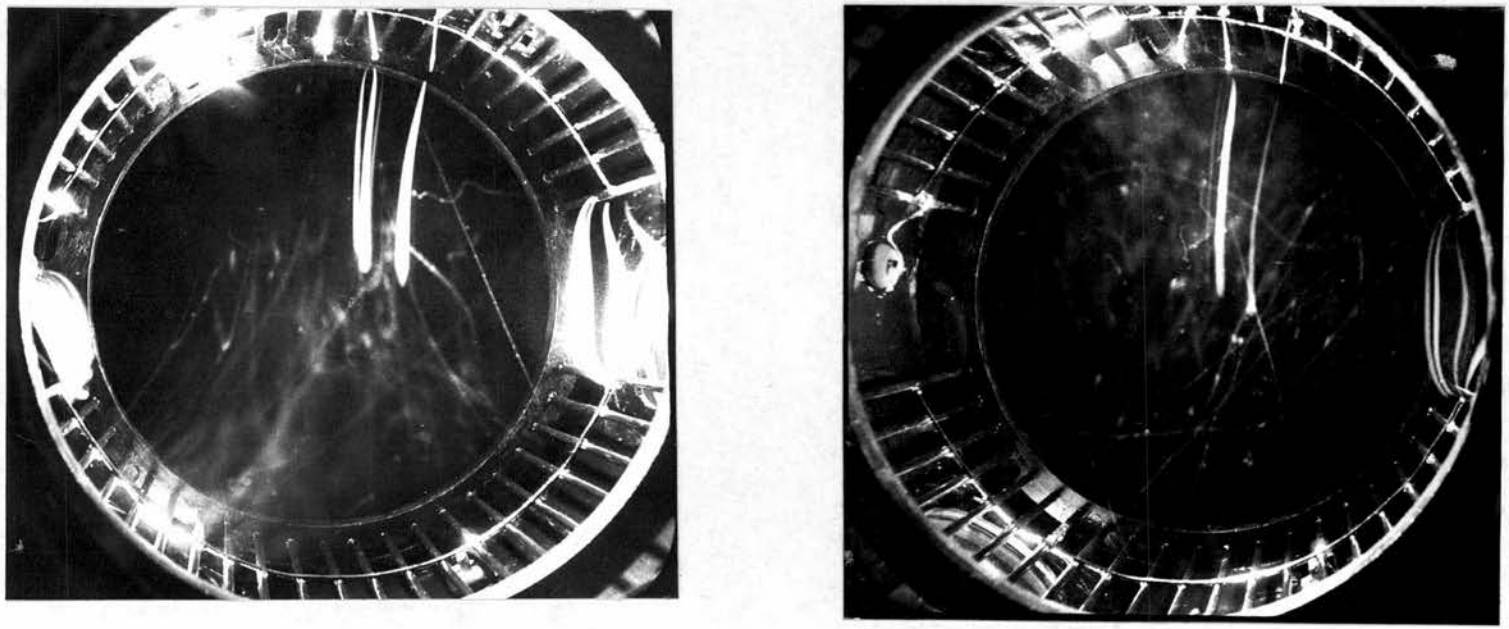

(a) (b)

PLATE 7.

(b) The mobility of the positive and negative ions is of the same order of magnitude. In plate 7 the clearing field, removed immediately before the expansion took place, was only applied for approximately 2 seconds. The clearing field voltages were $\pm$ 1350 volts and the field across the centre of the chamber was $\sim {}^{1700}/_{17}$ volts/cm. The ions have drifted $\sim$ 8 cms in 2 seconds so the mobility in argon at 50 atmos is 2 cms/sec/volt/cm. The mobility of heavy ions of mass number greater than 10 in pure argon is 2.8 - 3.8 cms/sec/volt/cm, but the presence of alcohol and oxygen will be expected to reduce this considerably. As the mobilities for negative and positive ions were observed to be of the same order of magnitude, the negative ions must consist of an electron attached to a neutral atom or molecule. A free electron would cross the chamber very much more rapidly but such electrons are not likely to be present because capture of free electrons (formed by ionisation of the atoms and molecules of the chamber gas) by a neutral alcohol or oxygen molecule or less frequently by an argon atom is expected to take place very soon after the electron is released.

(c) The discharge takes place at both positive and negative points ((a) and (b) respectively in plates 6 and 7). The cloud tracks appear to be denser in the case of positive points, but this may be due to

the preferential condensation of ethyl alcohol on positive ions. The absence of drop condensation in the region near the discharge points is likely to be due to the rapid motion of the ions away from this region before drop growth can take place.

Owing to the lack of experimental results, it is not possible to state the mode of formation of the ions in the present experiment. Experiments have been made to study these processes using cloud chambers[1] and other methods,[2] and the production of ions is considered to take place by at least two methods. Under the conditions of the present experiment ionisation by collision by heavy ions is not likely to take place and the two methods involve the production of unattached electrons.

Firstly in the case of discharge at a positive point, electrons are removed from negative ions by the high electric field in the neighbourhood of the discharge points and the free electrons are able to ionise many atoms before being captured to form a heavy ion or being collected at the anode. The positive ions are then free to drift across the chamber under the influence of the clearing field.

In the case of negative point discharges the process is not so clear. Positive ions attracted to a metal

surface tend to extract electrons from the surface and a continuous discharge can be set up.[3] It is not known if this process can take place at non-metallic surfaces such as cotton however, and without further experimental observation it is not possible to discover if this is the process taking place in the present experiment.

The discharges were eliminated during normal use of the chamber by making sure that there were no uninsulated regions on the electrode surfaces.

REFERENCES: Appendix II

(1) Allen et al. : Rev. Sc. Inst. 30, 230,1959.

(2) Llewellyn Jones et al.: Proc. Roy. Soc. A, 216, 267, 1953.

(3) " " " : Proc. Roy. Soc. A, 218, 88, 1953.

ACKNOWLEDGMENTS

I wish to thank Professor N. Feather, F.R.S., for the use of his laboratory facilities in the Department of Natural Philosophy. Grateful thanks are due to Dr. G.R. Evans for his advice and encouragement and for his having suggested the subjects of this thesis.

In addition thanks are extended to Dr. R.A. Donald, now at the University of Liverpool, for all his encouragement, and to Mr. A. Headridge and his staff for much valuable assistance in the construction of apparatus.

I am indebted to D.S.I.R. for the provision of a maintenance allowance.